

RADC-TR-81-352 Final Technical Report February 1982



APPLICATION OF PHASE RETRIEVAL

EIKONIX Corporation

Sponsored by Defense Advanced Research Projects Agency (DoD) ARPA Order No. 3655

APPROVED FOR PUBLIC RELEASE; DISTRIBUTION UNLIMITED

The views and conclusions contained in this document are those of the authors and should not be interpreted as necessarily representing the official policies, either expressed or implied, of the Defense Advanced Research Projects Agency or the U.S. Government

ROME AIR DEVELOPMENT CENTER
Air Force Systems Command
Griffiss Air Force Base, New York 13441



82 04 13 134

ITIC FILE COPY

This report has been reviewed by the RADC Public Affairs Office (PA) and is releasable to the National Technical Information Service (NTIS). At NTIS it will be releasable to the general public, including foreign nations.

RADC-TR-81-352 has been reviewed and is approved for publication.

APPROVED:

DORIS HAMILL, Capt, USAF

Project Engineer

Frank Mehm

APPROVED:

FRANK J. REHM

Technical Director Surveillance Division

FOR THE COMMANDER:

JOHN P. HUSS

Acting Chief, Plans Office

If your address has changed or if you wish to be removed from the RADC mailing list, or if the addressee is no longer employed by your organization, please notify RADC (OCSE) Griffiss AFB NY 13441. This will assist us in maintaining a current mailing list.

Do not return copies of this report unless contractual obligations or notices on a specific document requires that it be returned.

APPLICATION OF PHASE RETRIEVAL

Dr. Robert Gonsalves

Contractor: EIKONIX Corporation Contract Number: F30602-80-C-0186

Effective Date of Contract: 23 June 1980 Contract Expiration Date: 31 July 1981

Short Title of Work: Application of Phase Retrieval

Program Code Number: 0E20

Period of Work Covered: 23 June 80 - 31 July 81

Principal Investigator: Dr. Robert Gonsalves

Phone: 617-275-5070

Project Engineer: Capt Doris Hamill

Phone: 315-330-3148

Approved for public release; distribution unlimited

This research was supported by the Defense Advanced Research Projects Agency of the Department of Defense and was monitored by Doris Hamill, Capt, USAF (OCSE), Griffiss AFB NY 13441 under Contract F30602-80-C-0186.

UNCLASSIFIED

SECURITY CLASSIFICATION OF THIS PAGE (When Date Entered)

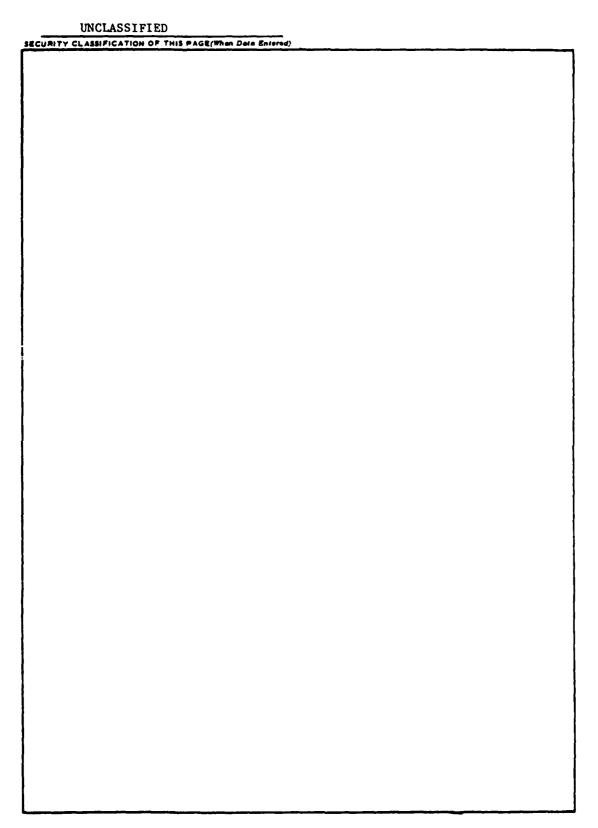
RADC-TR-81-352 APPLICATION OF PHASE RETRIEVAL APPLICATION OF PHASE RETRIEVAL T. AUTHOR(s) Dr. Robert Gonsalves S. TYPE OF REPORT A PERIOD COVERED Final Technical Report 23 Jun 80 - 31 Jul 81 EC(2112901) Final Technical Report 23 Jun 80 - 31 Jul 81 EC(2112901) Dr. Robert Gonsalves F30602-80-C-0186 S. PERFORMING ORGANIZATION NAME AND ADDRESS EIKOMIX Corporation 23 Crosby Drive Bedford MA 01730 10. CONTROLLING OFFICE NAME AND ADDRESS Defense Advanced Research Projects Agency 1400 Wilson Blvd ATLINGTON VA 22200 11. MONITORING AGENCY NAME & ADDRESS/II different from Controlling Office) ROME AIR Development Center (OCSE) Griffiss AFB NY 13441 12. DECLASSIFIED TS. ECCURITY CLASS. (st links report) Approved for public release; distribution unlimited 13. DISTRIBUTION STATEMENT (st links Report) Approved for public release; distribution unlimited 14. Supplementary Notes RADC Project Engineer: Doris Hamill, Capt, USAF 15. Supplementary Notes RADC Project Engineer: Doris Hamill, Capt, USAF	REPORT DOCUMENTATION PAGE	READ INSTRUCTIONS BEFORE COMPLETING FORM
APPLICATION OF PHASE RETRIEVAL APPLICATION OF PHASE RETRIEVAL APPLICATION OF PHASE RETRIEVAL 7. AUTHOR(s) Dr. Robert Gonsalves 5. PERFORMING ORGANIZATION NAME AND ADDRESS EIKONIX Corporation EIKONIX Corporation 23 Crosby Drive Bedford MA 01730 11. CONTROLLING OFFICE NAME AND ADDRESS Defense Advanced Research Projects Agency 1400 Wilson Blvd Arlington VA 22209 14. MONITORING AGENCY NAME & ADDRESS(it different from Controlling Office) Rome Air Development Center (OCSE) Griffiss AFB NY 13441 16. DISTRIBUTION STATEMENT (of the obstract entered in Block 20, It different from Report) Same 18. SUPPLEMENTARY NOTES RADC Project Engineer: Doris Hamill, Capt, USAF 19. KEY WORGS (Continue on reverse side if necessary and identify by block number) phase estimation phase estimation active mirrors phase sensing wavefront sensing	I .	O. 3. RECIPIENT'S CATALOG NUMBER
APPLICATION OF PHASE RETRIEVAL APPLICATION OF PHASE RETRIEVAL The state of the selection	RADC-TR-81-352	3 / - ²
APPLICATION OF PHASE RETRIEVAL 23 Jun 80 - 31 Jul 81 5. PERFORMING ORG. REPORT NUMBER EC/2/112901 7. AUTHOR(4) Dr. Robert Gonsalves F30602-80-C-0186 5. PERFORMING ORGANIZATION NAME AND ADDRESS EIKONIX Corporation 23 Crosby Drive Bedford MA 01730 11. CONTROLLING OFFICE NAME AND ADDRESS Defense Advanced Research Projects Agency 1400 Wilson Blvd Arlington VA 22209 14. MONITORING AGENCY NAME & ADDRESS(II different from Controlling Office) 15. SECURITY CLASS. (of this report) 16. DISTRIBUTION STATEMENT (of this Report) Approved for public release; distribution unlimited 17. DISTRIBUTION STATEMENT (of this abbitract entered in Block 20, II different from Report) Same 18. SUPPLEMENTARY NOTES RADC Project Engineer: Doris Hamill, Capt, USAF 19. KEY WORDS (Continue on reverse side if necessary and identify by block number) phase estimation active mirrors phase estimation active mirrors phase estimation active mirrors phase estimation active mirrors	4. TITLE (and Subtitle)	5. TYPE OF REPORT & PERIOD COVERED
7. AUTHOR(s) Dr. Robert Gonsalves S. PERFORMING ORGANIZATION NAME AND ADDRESS EIKONIX Corporation 23 Crosby Drive Bedford MA 01730 10. CONTROLLING OFFICE NAME AND ADDRESS Defense Advanced Research Projects Agency 1400 Wilson Blvd Arlington VA 22209 14. Monitoring Agency Name & ADDRESS(if different from Controlling Office) Rome Air Development Center (OCSE) Griffiss AFB NY 13441 16. DISTRIBUTION STATEMENT (of the abstract entered in Block 20, if different from Report) Same 18. Supplementary notes RADC Project Engineer: Doris Hamill, Capt, USAF	ADDITION OF DUASE DETRIBUAL	Final Technical Report
Dr. Robert Gonsalves F30602-80-C-0186 F30602-80-C-0186 F30602-80-C-0186 Dr. Robert Gonsalves F30602-80-C-0186 Dr. Robert Gonsalves F30602-80-C-0186 Dr. Robert Gonsalves F30602-80-C-0186 Dr. Robert Gonsalves Dr. Robert Gonsalves T0. PROGRAM ELEMENT, PROJECT, TASK ARR & WORK UNIT NUMBERS ARR & WORK UNIT NUMBERS C6550102 T1. CONTROLLING OFFICE NAME AND ADDRESS Defense Advanced Research Projects Agency 1400 Wilson Blvd Arlington VA 22209 T3. NUMBER OF PAGES T2. REPORT DATE February 1982 T3. NUMBER OF PAGES T2. REPORT DATE February 1982 T3. NUMBER OF PAGES T2. REPORT DATE February 1982 T3. NUMBER OF PAGES T2. REPORT DATE February 1982 T3. NUMBER OF PAGES T2. REPORT DATE February 1982 T3. NUMBER OF PAGES T2. REPORT DATE February 1982 T3. NUMBER OF PAGES T2. REPORT DATE February 1982 T3. NUMBER OF PAGES T3. NUMBER OF PAGES T3. NUMBER OF PAGES T3. SECURITY CLASS. (of this report) TS. DECLASSIFIED TS. DECLASSIFICATION/OWNGRADING N/A T3. DISTRIBUTION STATEMENT (of the abstract entered in Block 20, if different from Report) Same T4. SUPPLEMENTARY NOTES RADC Project Engineer: Doris Hamill, Capt, USAF T5. KEY WORDS (Continue on reverse side if necessary and identify by block number) phase estimation active mirrors phase sensing wavefront sensing	APPLICATION OF PRASE RETRIEVAL	
Dr. Robert Gonsalves F30602-80-C-0186 F20602-80-C-0186 F30602-80-C-0186 F30602-80-C-0186 F30602-80-C-0186 F20602-80-C-0186 F30602-80-C-0186 F30602-8		
Dr. Robert Gonsalves F30602-80-C-0186 PROGRAM LEWENT PROJECT TASK AREA & WORK UNIT HUMBERS EIKONIX Corporation 23 Crosby Drive Bedford MA 01730 10. CONTROLLING OFFICE NAME AND ADDRESS Defense Advanced Research Projects Agency 1400 Wilson Blvd Arlington VA 22209 18. MONITORING AGENCY NAME & ADDRESS/II different from Controlling Office) Rome Air Development Center (OCSE) Griffiss AFB NY 13441 16. DISTRIBUTION STATEMENT (of the abstract entered in Block 20, if different from Report) Same 17. DISTRIBUTION STATEMENT (of the abstract entered in Block 20, if different from Report) Same 18. SUPPLEMENTARY NOTES RADC Project Engineer: Doris Hamill, Capt, USAF	7 Autuogo	EC/2112901
9. Performing Organization name and address EIKONIX Corporation 23 Crosby Drive Bedford MA 01730 11. Controlling office name and address Defense Advanced Research Projects Agency 1400 Wilson Blvd Arlington VA 22209 14 Monitorians Agency American Address Address/ Indicate the Controlling Office) Rome Air Development Center (OCSE) Griffiss AFB NY 13441 16. Distribution statement (of this Report) Approved for public release; distribution unlimited 17. DISTRIBUTION STATEMENT (of this abstract entered in Block 26, 16 different from Report) Same 18. Supplementary notes RADC Project Engineer: Doris Hamill, Capt, USAF		o. Con Hazi on Gran Number(s)
23 Crosby Drive Bedford MA 01730 11. CONTROLLING OFFICE NAME AND ADDRESS Defense Advanced Research Projects Agency 1400 Wilson Blvd ATINGTON VA 22209 14. MONITORING AGENCY NAME & ADDRESS(If different from Controlling Office) Rome Air Development Center (OCSE) Griffiss AFB NY 13441 16. DISTRIBUTION STATEMENT (of this Report) Approved for public release; distribution unlimited 17. DISTRIBUTION STATEMENT (of the abstract entered in Block 20, If different from Report) Same 18. SUPPLEMENTARY NOTES RADC Project Engineer: Doris Hamill, Capt, USAF 19. KEY WORDS (Continue on reverse side if necessary and identify by block number) phase estimation active mirrors phase sensing wavefront sensing	Dr. Robert Gonsalves	F30602-80-C-0186
23 Crosby Drive Bedford MA 01730 11. CONTROLLING OFFICE NAME AND ADDRESS Defense Advanced Research Projects Agency 1400 Wilson Blvd ATINGTON VA 22209 14. MONITORING AGENCY NAME & ADDRESS(If different from Controlling Office) Rome Air Development Center (OCSE) Griffiss AFB NY 13441 16. DISTRIBUTION STATEMENT (of this Report) Approved for public release; distribution unlimited 17. DISTRIBUTION STATEMENT (of the abstract entered in Block 20, If different from Report) Same 18. SUPPLEMENTARY NOTES RADC Project Engineer: Doris Hamill, Capt, USAF 19. KEY WORDS (Continue on reverse side if necessary and identify by block number) phase estimation active mirrors phase sensing wavefront sensing		10. PROGRAM ELEMENT, PROJECT, TASK
Bedford MA 01730 11. CONTROLLING OFFICE NAME AND ADDRESS Defense Advanced Research Projects Agency 1400 Wilson Blvd ATlington VA 22209 14. MONITORING AGENCY NAME & ADDRESS(II different from Controlling Office) Rome Air Development Center (OCSE) Griffiss AFB NY 13441 16. DISTRIBUTION STATEMENT (of this Report) Approved for public release; distribution unlimited 17. DISTRIBUTION STATEMENT (of the abstract entered in Block 20, If different from Report) Same 18. SUPPLEMENTARY NOTES RADC Project Engineer: Doris Hamill, Capt, USAF 19. KEY WORDS (Continue on reverse side if necessary and identify by block number) phase estimation active mirrors phase sensing wavefront sensing	•	1
Bedford MA 01/30 11. CONTROLLING OFFICE NAME AND ADDRESS Defense Advanced Research Projects Agency 1400 Wilson Blvd Arlington VA 22209 13. NUMBER OF PAGES 122 14. MONITORING AGENCY NAME & ADDRESS/II different from Controlling Office) Rome Air Development Center (OCSE) Griffiss AFB NY 13441 15. DISTRIBUTION STATEMENT (of this Report) Approved for public release; distribution unlimited 17. DISTRIBUTION STATEMENT (of the ebetrect entered in Block 20, If different from Report) Same 18. SUPPLEMENTARY NOTES RADC Project Engineer: Doris Hamill, Capt, USAF 19. KEY WORDS (Continue on reverse side if necessary and identify by block number) phase estimation active mirrors phase sensing wavefront sensing		C6550102
Defense Advanced Research Projects Agency 1400 Wilson Blvd AT1Ington VA 22209 14. MONITORING AGENCY NAME & ADDRESS/II different from Controlling Office) Rome Air Development Center (OCSE) Griffiss AFB NY 13441 16. DISTRIBUTION STATEMENT (of this Report) Approved for public release; distribution unlimited 17. DISTRIBUTION STATEMENT (of the ebetrect entered in Block 20, if different from Report) Same 18. SUPPLEMENTARY NOTES RADC Project Engineer: Doris Hamill, Capt, USAF 19. KEY WORDS (Continue on reverse side if necessary and identify by block number) phase estimation active mirrors phase sensing wavefront sensing		
1400 Wilson Blvd Arlington VA 2209 14. MONITORING AGENCY NAME & ADDRESS/II different from Controlling Office) Rome Air Development Center (OCSE) Griffiss AFB NY 13441 15. DECLASSIFIED 15. DECLASSIFICATION/DOWNGRADING SCHEDULE 16. DISTRIBUTION STATEMENT (of this Report) Approved for public release; distribution unlimited 17. DISTRIBUTION STATEMENT (of the obstract entered in Block 20, if different from Report) Same 18. SUPPLEMENTARY NOTES RADC Project Engineer: Doris Hamill, Capt, USAF 19. KEY WORDS (Continue on reverse side if necessary and identify by block number) phase estimation active mirrors phase sensing wavefront sensing		
ATTINGTON VA 22209 14. MONITORING AGENCY NAME & ADDRESS/II different from Controlling Office) Rome Air Development Center (OCSE) Griffiss AFB NY 13441 16. DISTRIBUTION STATEMENT (at this Report) Approved for public release; distribution unlimited 17. DISTRIBUTION STATEMENT (at the ebetrect entered in Block 20, if different from Report) Same 18. SUPPLEMENTARY NOTES RADC Project Engineer: Doris Hamill, Capt, USAF 19. KEY WORDS (Continue on reverse side if necessary and identify by block number) phase estimation active mirrors phase sensing wavefront sensing	,	
Rome Air Development Center (OCSE) Griffiss AFB NY 13441 The Distribution statement (of this Report) Approved for public release; distribution unlimited 17. DISTRIBUTION STATEMENT (of the abstract entered in Block 20, if different from Report) Same 18. Supplementary notes RADC Project Engineer: Doris Hamill, Capt, USAF 19. KEY WORDS (Continue on reverse side if necessary and identify by block number) phase estimation active mirrors phase sensing wavefront sensing		
Rome Air Development Center (OCSE) Griffiss AFB NY 13441 16. Distribution Statement (of this Report) Approved for public release; distribution unlimited 17. Distribution Statement (of the ebetrect entered in Block 20, if different from Report) Same 18. Supplementary notes RADC Project Engineer: Doris Hamill, Capt, USAF 19. KEY WORDS (Continue on reverse side if necessary and identify by block number) phase estimation active mirrors phase sensing wavefront sensing	14. MONITORING AGENCY NAME & ADDRESS(If different from Controlling Office)	15. SECURITY CLASS, (at this report)
16. DISTRIBUTION STATEMENT (of this Report) Approved for public release; distribution unlimited 17. DISTRIBUTION STATEMENT (of the obstract entered in Block 20, if different from Report) Same 18. SUPPLEMENTARY NOTES RADC Project Engineer: Doris Hamill, Capt, USAF 19. KEY WORDS (Continue on reverse side if necessary and identify by block number) phase estimation active mirrors phase sensing wavefront sensing	Rome Air Development Center (OCSE)	
Approved for public release; distribution unlimited 17. DISTRIBUTION STATEMENT (of the ebetrect entered in Block 20, if different from Report) Same 18. SUPPLEMENTARY NOTES RADC Project Engineer: Doris Hamill, Capt, USAF 19. KEY WORDS (Continue on reverse side if necessary and identify by block number) phase estimation active mirrors phase sensing wavefront sensing	Griffiss AFB NY 13441	154. DECLASSIFICATION/DOWNGRADING SCHEDULE
17. DISTRIBUTION STATEMENT (of the abstract entered in Block 20, if different from Report) Same 18. SUPPLEMENTARY NOTES RADC Project Engineer: Doris Hamill, Capt, USAF 19. KEY WORDS (Continue on reverse side if necessary and identify by block number) phase estimation active mirrors phase sensing wavefront sensing	16. DISTRIBUTION STATEMENT (of this Report)	A-1-1-1-1
Same 18. SUPPLEMENTARY NOTES RADC Project Engineer: Doris Hamill, Capt, USAF 19. KEY WORDS (Continue on reverse aide if necessary and identify by block number) phase estimation active mirrors phase sensing wavefront sensing	Approved for public release; distribution unli	lmited
RADC Project Engineer: Doris Hamill, Capt, USAF 19. KEY WORDS (Continue on reverse side if necessary and identify by block number) phase estimation active mirrors phase sensing wavefront sensing	17. DISTRIBUTION STATEMENT (of the ebetrect entered in Block 20, if different in	rom Report)
RADC Project Engineer: Doris Hamill, Capt, USAF 19. KEY WORDS (Continue on reverse aide if necessary and identify by block number) phase estimation active mirrors phase sensing wavefront sensing	Same	
19. KEY WORDS (Continue on reverse side if necessary and identify by block number) phase estimation active mirrors phase sensing wavefront sensing	IS. SUPPLEMENTARY NOTES	
phase estimation active mirrors phase sensing wavefront sensing	RADC Project Engineer: Doris Hamill, Capt, US	SAF
phase sensing wavefront sensing	19. KEY WORDS (Continue on reverse side if necessary and identify by block number	(*)
phase retrieval	phase sensing wavefront sensing	
	phase retrieval	

20. ABSTRACT (Continue on reverse side if necessary and identity by block number)

The purpose of this study was to determine how the phase retrieval algorithm developed under previous contract, worked in the face of real world constraints. The problems of finite detector size, noise in the measurements, and non-point objects were handled analytically, experimentally, and by blind testing. No significant problems were uncovered.

DD 1 JAN 73 1473 EDITION OF 1 NOV 65 IS OBSOLETE

UNCLASSIFIED
SECURITY CLASSIFICATION OF THIS PAGE (Phon Data Entered)



1 INTRODUCTION

The objective of this study is to demonstrate the utility of the phase retrieval concept for determining the wavefront aberrations of an optical system from image intensity data. Phase retrieval techniques use only the focal plane detector array to estimate the wave aberration function θ of an active optical system. The estimate would then be used to derive control signals to align or maintain alignment of the optical system. See Figure 1.

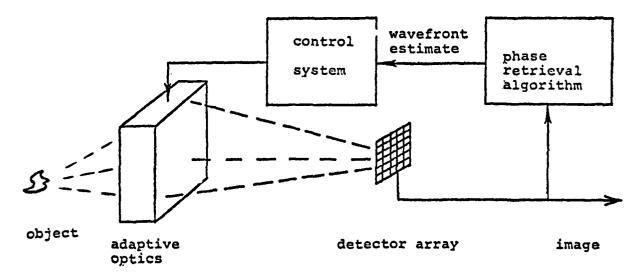
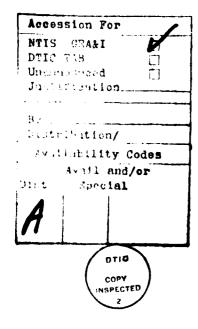


Figure 1. Phase retrieval in an adaptive imaging system

In a previous study (F30602-77-C-0176) we showed that phase retrieval is a promising technique to maintain alignment of an active optical system. However, most of the study was theoretical in nature and the best results were obtained with point sources, little or no noise on the detector output, and adequately sampled data (at or higher than the Nyquist sampling rate). In this follow-on effort we are charged to thoroughly simulate the algorithm's performance, particularly with respect to noise, undersampling (because of the finite detector size), and extended objects. We are also charged to show how phase retrieval can be developed into a system level proof-of-concept demonstration, where the system is to be specified by the government.

In this report we review the phase retrieval concept, show the effects of undersampling and noise, present algorithms for extended objects, show several ways in which the algorithm can be speeded up, introduce the concept of phase diversity imaging (as a research by-product of our extended object algorithm), give results of an experiment that attempts to verify the extended object concept, and present the results of a series of blind tests of the phase retrieval algorithm when the data is noisy and undersampled.



2 REVIEW OF THE PHASE RETRIEVAL CONCEPT

When a monochromatic point object is imaged through an optical system, the observable is the point spread function (PSF) p(x). The PSF is the modulus squared of the coherent system function h(x),

$$p(x) = |h(x)|^2.$$

The Fourier transform of h(x),

$$H(f) = \int_{-\infty}^{\infty} h(x) \exp(-i2\pi f x) dx,$$

is the coherent system function of the optical system. Its modulus, A(f), is a zero-one function, corresponding to the pupil function, and its phase $\theta(f)$ is proportional to the aberrated wavefront across the aperture. Thus,

$$H(f) = A(f) \exp(i\theta(f)).$$

Although we use a one-dimensional representation in this discussion, the results are valid for the physical, two-dimensional problem, except as noted.

Concisely stated, the phase retrieval concept is to estimate $\theta(f)$ based on observation of p(x).

The basic algorithm uses a polynomial expansion for $\theta(f)$,

$$\theta(f) = \sum_{k=1}^{\infty} c_k \theta_k(f)$$

where $\{\theta_k(f)\}$ is a suitable set of f-polynomials. A phase estimate $\hat{\theta}(f)$ with a finite number of c_k 's is formed and an estimated OTF, $P_C(f)$, is calculated. This is compared to the measured OTF, P(f),

and an error metric drives a C-vector search to minimize the error. When the error reaches a stable minimum we declare $\hat{\theta}(f)$ to be the estimate of $\theta(f)$. See Figure 2.

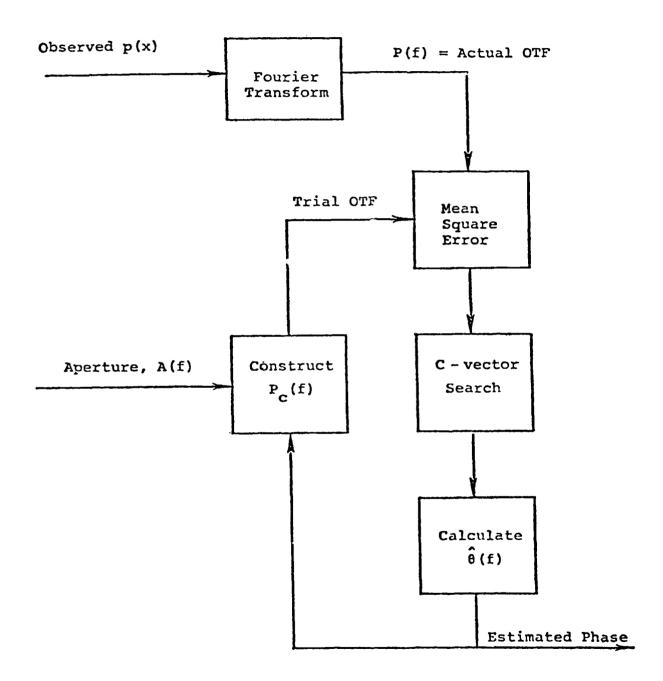


Figure 2 Farameter Search Algorithm

An example of phase retrieval which uses the basic algorithm is shown in Figures 3, 4, and 5. Figure 3 is a contour plot of the phase aberration (about 2 waves, peak-to-valley) across a circular, unobscurated aperture. This yields the PSF shown in Figure 4. When we estimate the phase from Figure 4 and subtract this estimate from the actual phase in Figure 3, the resulting PSF is nearly diffraction limited, as shown in Figure 5.

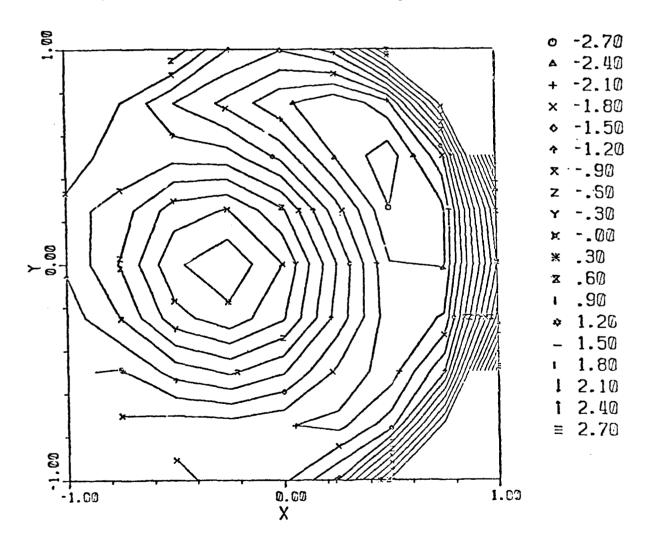


Figure 3 Initial phase aberration across exit pupil. Contour values in waves.

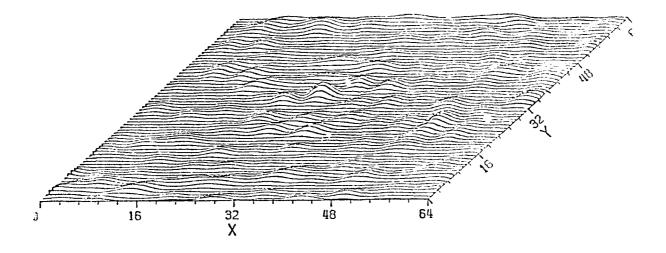


Figure 4 PSF of original aberrated system. Point detectors.

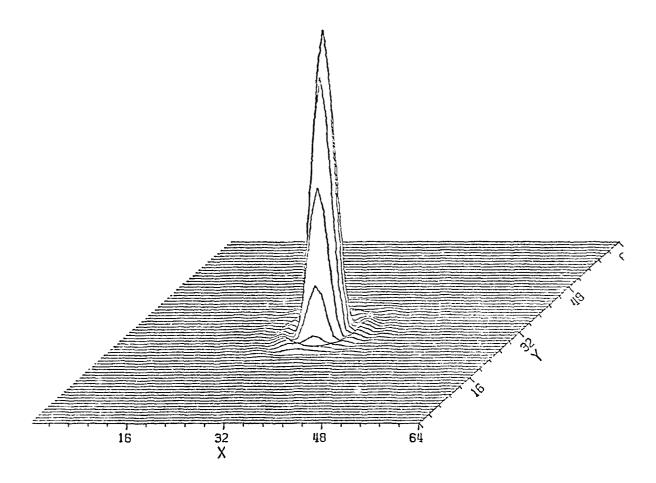


Figure 5 PSF after correction. Point detectors.

Details on the algorithm that implements the phase retrieval concept are given in the final report on the previous contract. These details include discussions of the search technique (a grid search followed by a modified, steepest descent algorithm of the Fletcher-Powell type), the numerical procedures for calculating the PSF, the polynomials (Zernicke polynomials, to order 24), and the computer code itself. The final report also describes successful blind tests of the algorithm that were conducted with Draper Labs and with Hughes Aircraft Company; it describes a simple experimental verification of the theory (point source, aberrated by a phase-distorted imaging system); and it gives some preliminary results on extended objects.

3 ALIASING

An array of detectors in the focal plane spatially averages the image over the detector profile of each individual detector and produces an array of numbers that describes a sampled image. The sampling interval is the spacing between detectors, measured from center-to-center. If the image a(x) is band-limited to a spatial frequency $f_{\rm max}$ (cycles per unit distance), then a(x) is completely determined if spatial samples are taken at intervals smaller than $1/(2\ f_{\rm max})$, the Nyquist sampling interval. In what follows we will set $f_{\rm max}$ equal to $1/(\lambda F \#)$, as is the case for a diffraction-limited optical system.

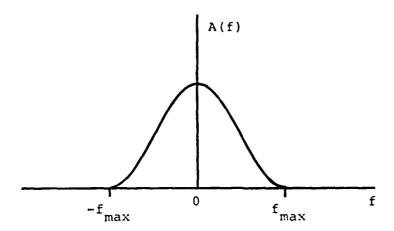
For the purposes of this study we assume that the diode spacing will be up to five times <u>larger</u> than the Nyquist sampling interval. Thus, the image will be undersampled and there will be a severe amount of "aliasing". This aliasing effect is described as follows. If the image is a(x) with Fourier transform A(f), the sampling procedure produces a spectrum G(f),

$$G(f) = \sum_{k=-\infty}^{\infty} A(f - kf_0),$$

where

$$x_0 = 1/f_0$$

is the spatial sampling interval. If f_0 is less than twice the highest frequency in A(f), the aliases in G(f) overlap and the spectrum A(f) (and, therefore, a(x)) cannot be recovered. See Figure 6.



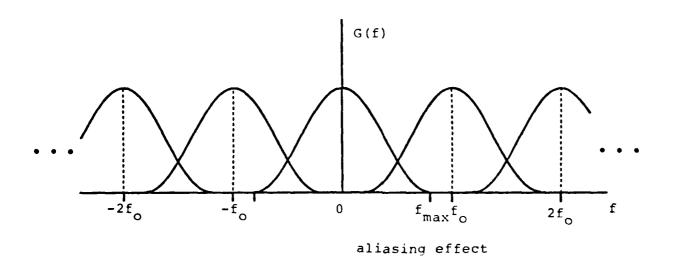


Figure 6. The aliases overlap if $f_0 < 2f_{max}$.

The effects of undersampling are more graphic when shown in the spatial domain. Thus, Figure 7 shows a digital image of a point spread function sampled at the Nyquist sampling rate. This PSF is the result of about one wave (peak-to-peak) of wavefront distortion in the aperture. In Figure 8 we show another PSF with approximately the same amount of wavefront distortion. But this has been sampled by detectors that are four times larger than the Nyquist sampling rate. Note the loss of detail.

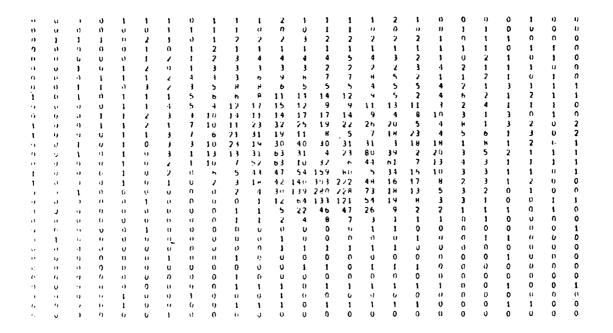


Figure 7. Part of a 32 by 32 point spread function sampled at the Nyquist sampling rate



Figure 8. 8 by 8 detected point spread function undersampled by a factor of 4 in both X and Y directions

This example illustrates the concern for the utility of a phase retrieval algorithm when the detectors are large. The image data is grossly washed out. It turns out, however, that the phase associated with the PSF of Figure 8 was accurately captured by the algorithm, even when a small amount of noise is added to the observed PSF.

In order to study the effects of aliasing on phase retrieval, a new computer program was written which works on PSF's instead of OTF's. Square blocks of pixels may be summed into one output pixel, simulating the effect of using square detectors that are an integral number of samples wide. The initial, unaliased PSF is sampled at the Nyquist interval of $\lambda F\#/2$. The pupil is a circular aperture in a 16 by 16 array, as shown in Figure 9. A phase aberration is constructed over the aperture and the generalized pupil function computed. It is buffered out to 32 by 32 and a Fast Fourier Transform taken, resulting in a 32 by 32 coherent spread function. The magnitude squared gives the PSF.

```
4 0 0 0 0 0 0 4
                      Ú
     0 0 0 0 0
              0 0 0 0
440000000
                 0 0 0
                      0
                        0
4 0 0 0 0 0 0 0 0
                 000000
4 0 0 0 0 0 0 0 0 0 0 0 0 0 0
0 0 0 0 0 0 0 0 0 0 0 0 0 0 0 0
0000000000000000
0 0 0 0 0 0 0 0 0 0 0 0 0 0 0
0 0 0 0 0 0 0 0 0 0 0 0 0 0 0 0
0 0 0 0 0 0 0 0 0 0 0 0 0 0 0 0
0 0 0 0 0 0 0 0 0 0 0 0 0 0 0 0
4 0 0 0 0 0 0 0 0 0 0 0 0 0 0 4
4 0 0 0 0 0 0 0 0 0 0 0 0 0 0 4
4 4 0 0 0 0 0 0 0 0 0 0 0 0 4 4
  4 4 0 0 0 0 0 0 0 0 0 0 0 4 4 4
   4 4
       4000000444
```

Figure 9. Pupil function used in simulations.
0 indicates inside aperture, 4 indicates outside aperture.

Simulations were run by reading in an aberration (in terms of Zernicke polynomials) and constructing a PSF. The detector model was applied and noise added. This is the simulated measured PSF. The program attempts to deduce the aberrations by searching over the parameters which are the coefficients of the Zernicke polynomials to find a PSF which yields the best possible fit to the measured PSF. The error metric is

$$E(\vec{p}) = \sum_{i,j} (P_{ij}(\vec{p}) - D_{ij})^2,$$

where D is the measured PSF data and P the trial PSF, which is a function of the parameters \vec{p} .

The Zernicke polynomials used are shown in Table 1. The results for various noise levels and amounts of aliasing are presented in Table 2. The row labelled "initial" is the aberration corresponding to the simulated measured PSF. This aberration across the aperture is shown in Figure 10. Cases 1 through 7 all used detectors which were averages of a 4 by 4 array of the original Nyquist sampled pixels. Figure 7 shows the Nyquist sampled 32 by 32 PSF from the initial aberration. Figure 8 shows the 8 by 8 detected PSF. In Figure 11 is the noisy PSF from case 2.

Table 1
Zernicke Polynomials

Number	Form	Name
2	×	x tilt
3	У	y tilt
4	x^2+y^2	focus
5	x^2-y^2	0° astigmatism
6	2xy	45° astigmatism
7	$\times (r^2-3)$	x coma
8	y(r ² -3)	y coma

<u> </u>	0								
24.4	Ratio	.30	06.	66.	. 95	. 95	.83	. 85	.54
SWZ	Phase	.224	.051	.019	.036	.035	.070	.063	.119
ise Standard Deviation	Peak		0.	1.03%	2.06%	2.06%	4.12%	4.12%	8.25%
Noise Devi	Peak		0.	.468	. 918	.918	1.82%	1.82%	3.65%
	8	. 05	.051	.035	.015	.017	034	800	140
Coefficient	7	3	313	312	316	292	321	290	325
	9	٦.	.104	960•	.097	.120	.127	.143	.224
Polynomial	5	.15	.156	.169	.182	.145	.198	.140	.234
1 1	4	.3	.293	.290	.280	.309	.247	.310	.267
Zernicke	3	0.	006	023	043	025	085	050	110
	2	0.	660.	017	030	055	033	760.	.148
00.5	case	Initial	-	2	я	4	iΩ	9	7

Results of Phase Retrieval when the PSF is undersampled by a factor of 4 in both X and Y directions Table 2

•	000.0	0.000	0.00	000.0	0.541	9.463	0.429	0.428	0.450	0.484	0.000	000.0	0.000	0000	000.0
0.00	00000	00000	0.638	0.465	0.356	0.301	0.289	0.310	0.353	0.407	0.461	0.507	00000	00000	00000
0.00	00000	0.674	0.447	0.295	0.206	0.170	0.177	0.215	0.275	0.346	0.417	0.478	0.518	00000	00000
0.000	0.799	0.506	0.296	0.161	0.00	0.068	0.000	0.143	0.216	0.301	0.384	0.457	0.509	0.528	00000
0.000	0.657	0.379	0.183	0.061	0.001	-0.007	0.026	0.090	0.174	0.268	0.361	0.443	0.502	0.529	00000
0.921	0.559	0.291	0.106	-0.006	-0.057	-0.057	-0.015	0.056	0.147	0.247	0.346	0.432	0.497	0.527	0.515
0.856	0.502	0.242	0.064	-0.043	-0.088	-0.082	-0.037	0.039	0.133	0.236	0.337	0.425	0.490	0.521	0.508
0.634	0.485	0.228	0.053	-0.050	-0.093	-0.086	-0.039	0.036	0.130	0.233	0.332	0.418	0.481	0.509	0.492
0.853	0.505	0.249	0.074	-0.030	-0.075	-0.070	-0.025	0.047	0.138	0.235	0,330	0.411	0.467	0.489	0.465
0.912	0.562	0.302	0.124	0.015	-0.034	-0.035	0.003	0.069	0.153	0.243	0.329	0.400	0.447	0.459	0.424
1.009	0.652	0.386	0.200	0.084	0.026	0.017	0.045	0.101	0.174	0.252	0.327	0.386	0.420	0.417	0,369
00000	0.775	0.499	0.303	0.175	0.105	0.084	0.099	0.141	0.199	0.263	0.322	0,365	0.382	0.363	00000
0.000	0.929	0.640	0.429	0.286	0.201	0.163	0.162	0.187	0.227	0.273	0,313	0.336	0.333	0.293	00000
0.000	00000	0.805	0.577	0.416	0.312	0.254	0.233	0.237	0.256	0.280	0.297	0.298	0.272	0000	00000
00000	00000	00000	0.745	0.562	0.436	0.355	0.310	0.290	0.285	0.283	0.274	0.248	000.0	000.0	000.0
00000	00000	00000	00000	00000	0.571	0.464	0.392	0.344	0.310	0.279	00000	0000	00000	00000	000.0

Figure 10 Phase aberations used in simulations, evaluated across the aperture, in units of waves.

10	10	10	0	2	Û	8	9
2	-2	12	15	21	12	1	0
2	2	20	61	50	22	6	0
11	5	8	116	104	32	1	13
1	10	6	159	448	9	12	3
4	5	-3	3	30	5	0	-2
-7	5	5	0	7	0	3	5
5	3	6	-3	0	2	-5	2

Figure 11 Noisy Detected Point Spread Function from Case 2.

The noise is added to each pixel of the detected PSF, and is independent and Gaussian distributed. The standard deviation of the noise is expressed in two ways in Table 2; as a percentage of the peak value of a diffraction-limited PSF as detected, and of the peak of the aberrated detected PSF. Cases 3 and 4, and 5 and 6, have the same noise levels but have different random realizations.

The parameter values listed in each row are the values at which the search terminated, and is the final estimate. When the initial parameters are corrected by the estimate, the residual phase aberration has an RMS value across the aperture as listed in the column labelled "RMS Phase". The Strehl ratio of the corrected, Nyquist sampled PSF is in the column labelled "Strehl Ratio". Not surprisingly, the quality of the final corrected PSF deteriorates as the noise level increases, until case 7 which results in only slight improvement.

From the results in Table 2 we see that a PSF, undersampled by a factor of 4, can provide a good estimate of the wavefront. The PSF has additive noise to a level of about 2% of the diffraction-limited peak.

Table 3 shows, for the same initial aberration the results of increasing the detector size. Even with 10 by 10 detectors, phase retrieval is still successful. Figure 12 shows the detected and noisy detected PSF's for case 13, with the 10 by 10 detectors. Table 3 lists, in the rows labelled "G" and "D", where the grid search terminated and the final result where the Davidon search finished.

Table 4 shows two different aberrations. Cases 14, 15, and 16 are for a detector size of 10 by 10. The noise-free case worked, and the noisest case resulted in significant improvement, while the less noisy one essentially failed in the grid search to find a good starting point for the Davidon search. Cases 17 and 18 show another aberration failing with 5 by 5 detectors, both for noise-free and noisy data. With 2 by 2 or 4 by 4 detectors, phase retrieval was successful.

These results show that aliasing is not a major problem to phase retrieval. There are still problems with regard to doing a fine enough mesh on the grid search to insure detection of the global minimum, but aliasing does not seem to create any new difficulties.

5	42	11	1	0		
5	366	33	1	0		
2	21	3	0	0		
0	1	1	0	0		
0	0	0	0	0		
1017	IAL F	SF	DET	ECTED	WITH	NOISE)
7	44	22	13	10		
14	363			13		
5	25	3	23	-17		
-6	4	23	-1	14		
B	16	• •	-12			

Figure 12 Case 13 Point spread functions (10 by 10 detector size)

)etector size	tor		92	rnicke	Polynom	nial Coe	Polynomial Coefficient		Noise S Devided	ise Standard Deviation Aberrated	RMS	Strch
Case			2	3	4	5	9	7	8	Peak	Peak	Phase	Ratio
Initial			0.	0.	. 3	.15	.1	3	ج0٠			. 224	.36
	.	ပ			.250	.125	.125	375	0.				
c 	n 	a	.035	.014	.264	.094	.097	-,365	.027	. 45%	.79%	.044	.93
		ပ			.250	.125	.01	375	0.				
	·	۵	070.	052	.263	.151	.110	344	.068	.43%	.72%	.051	06.
		Ŋ			.250	.250	.125	250	.125				
2		<u> </u>	.025	.035	.263	.162	.159	346	.051	.418	.69	.043	.93
75	c	S			.375	.125	.125	250	0.				
77	0	Q	024	.030	.339	.120	980.	271	.031	.418	.90%	.035	.95
2		5			.375	.125	.125	125	125				
7	-	۵	0.	.063	.366	920.	.102	268	.042	1.65%	3.6%	090	.87
-	-	O			.250	.125	0.	375	.125				
F T	- 	a	.037	015	.259	.043	022	393	.063	2.5%	3.168	.082	.76

Table 3 Results of Phase Retrieval for Various Detector Sizes

Strehl	Ratio				.78		.94		.38	-20		.21		.20		966.		666.
RMS	Phase		707		860.		.040		.160	.298		.227		.235		.010		.004
Noise Standard Deviation DL Aberrated	Peak				4.26%	C	•		2.13%			4.48	Ċ	,	c	•	C	
Noise Devi	Desire	4112			1.62%		•		.818			96.	c	•	C	•		•
	3	3	. 23	.125	.196	.250	.221	.125	004	. 29	.375	.406	.375	.393	.375	.291	.375	.291
Zornicke Polynomial Coefficient	· ·	,	-1-	.125	.126	.125	.105	0.	.065	. 20	.375	.414	.375	.406	.125	.199	.125	.200
nial Coc		٥	.34	.375	.359	.375	.390	. 625	.626	.19	. 625	.582	. 625	.558	.250	.179	.250	.186
Polynon	,	2	.08	0.	.032	.125	.130	0.	.032	.02	0.	.085	0.	920.	.125	.020	0.	.019
crnicke		7	.17	.250	.043	.125	.132	.125	.177	. 43	.250	.225	.250	.178	.375	.424	.375	.429
Z		3	Э.		.064		.022		.071	0		015		064		010		002
		:]	G		.1.18		011		087	0.		.031		031		013		006
tor	:			U	G	9	۵	ß	2		ß	۵	9	Ω	5	C.	5	2
Detector	;				10		0		10			S		'n		7		**
	3	', albe	11111111		7		15		16	Initial		17		œ		19		50

Table 4 Results of Phase Retrieval

4 NOTES ON EFFICIENT SEARCH TECHNIQUES

Previously proposed phase retrieval search methods have involved comparing a measured PSF (or, equivalently, an OTF) with a large number of PSF's from a grid of parameter values covering the region of parameter space which is expected to include the actual aberration. These PSF's have always been recomputed for each search, even though they do not change. A faster method, which actually uses less computational hardware, is to compute the PSF's once and store them on disk, and retrieve them as needed during the search.

To work out the speed of this operation, suppose that we wish to examine, in the grid search, three values for each of thirteen parameters. This yields 1.6 x 10⁶ PSF's. (Five values for nine parameters gives a slightly larger number.) Storing an eight by eight PSF, quantized to 256 levels (so that each pixel will fit ir a single byte) for each grid point would take 102 megabytes, which is within the capacity of a single large disk drive. If the data is read off the disk in an optimum manner so as not to waste disk head movements, three minutes are taken to transfer all the data to the CPU. To compute the error metric on a 64 pixel PSF takes 128 additions and 64 multiplications. The total for all 1.5 \times 10⁶ PSF's is $192 \cdot 10^6$ additions and $96 \cdot 10^6$ multiplications. To perform the computation in three minutes of disk read time requires a speed of 500 nsec per addition and 1000 nsec per multiplication. This is within the capability of a PDP 11/70 doing integer arithmetic. (Floating point is not needed for these calculations.) Since the CPU would be active at the same time as the disk transfer were taking place, the computation time and I/O time could be totally overlapped so that only three minutes are required for the entire search.

There remains the problem of the second grid search. This is performed at half the grid spacing of the first search in the region immediately around the best points of the first search. It has proven necessary only occasionally to actually do the second grid search in the simulations that have been run previously, but for higher dimensions of parameter space the distance from a point in the center of any hypercube formed by the grid points grows as the square root of the dimensionality. Prestoring PSF's calculated for parameter values on a finer grid mesh would take far too much storage. Calculating them as needed for a second grid search would dwarf the time of the first search. If the first grid spacing is small enough, then the second search can be avoided. Alternatively, a downhill search can be started from each of the best survivors of the first search. The downhill search time rises only linearly with the dimensionality.

A faster method for the first grid search involves the use of moments, or some other characterization of distinctive properties of the PSF. Five moments, as we use in Section 5, seem a good number. The PSF's used for the first grid search are sorted on their moments, into 15 bins adjusted for each moment to span the range of moment values, and perhaps so that approximately equal numbers of PSF's fall into each bin. The PSF's are placed on the disk in an order beginning with the PSF's where moments all fall into the first bins, stepping through all bins on the fifth moment, then moving onto the second bin of the fourth moment and stepping through all fifth moment bins, and cortinuing until the PSF's in the fifteenth bin for all moments are written. This order is listed in Table 5.

TABLE 5
Order of PSF's Sorted in Moments

$^{\rm M}$ 1	^M 2	м ₃	M ₄	^M 5
1	1	1	1	1
1	1	1	1	2
	•	• • •		•
1	1	1	1	15
1	1	1	2	1
		• • •		
1	1	1	2	15
		• • •		
1	1	1	15	15
1	1	2	1	1
15	15	15	15	15

This is a total of 15^5 , or 759,375 possible slots for a PSF to be assigned to. If we have 3¹³ grid points, or 1,594,323, there will be an average of two PSF's in each slot, although considerable variation may be expected. Given a measured PSF, its five moments may be calculated and a decision made as to which bin each moment falls in, in negligible time. A way of pointing to the area on disk which holds the PSF's corresponding to the five moments is needed. a table, with 759,375 entries may be constructed. Its size is such that it too must be on disk. Each table entry holds an address on the disk for where PSF data begins for that particular slot. Data continues on the disk until the next address in the table is reached. Access into table is easily computable; if the bin values for each moment are i, j, k, ℓ , and m, then element number $(i-1)*15^4 + (j-1)*15^3$ + $(k-1)*15^2$ + $(\ell-1)*15$ + m is the proper table address. Generating the sorted PSF file and the address table will require a great deal of computer time, but it only needs to be done once.

Examining only the bins into which the moments of measured PSF fall is unwise, since noise and the presence of other aberrations will perturb the moments. A safer course is to examine 'hree bins for each moment, the one into which the measured moment falls and the ones on either side. This corresponds to 20% of the range of moment values for each moment. For five moments, only .00032 of the full set of grid points survive. Taking three bins for each moment results in making 3⁵, or 243, references in the address table, which will point to, on the average, a total of 486 PSF's. Each of these PSF's may be compared with the measured PSF and a metric computed. This should take less than 30 seconds to do. Downhill searches can be started from the parameter sets associated with the PSF's with the lowest metrics. The parameters from the search that terminates at the smallest metric are the final estimate.

5 THE USE OF MOMENTS TO SPEED UP THE ALGORITHM

The search method which has been used for phase retrieval applications consists of an initial search over a rectangular grid of points in parameter space, a second search around the best (lowest metric) grid points at half the first grid spacing, and a downhill Davidon search from the best point of the second grid search. The initial grid search is the most crucial to obtaining a good phase estimate, and is quite time-consuming to compute the metric of the sum of the squares of the differences between the measured and trial PSF's point by point.

A method was sought that would allow, by means of a quick comparison of only a very few numbers associated with each PSF, whether or not a trial PSF is worthy of further consideration. A natural approach is to use moments of the PSF distribution. The most fundamental moment is the center of gravity, defined by

$$E = \int P(x,y) dxdy$$

$$x_{c.g.} = \int x P(x,y) dxdy/E$$

$$y_{c.g.} = \int y P(x,y) dxdy/E.$$

Given that the ideal position of the point object is known, the location of the c.g. (in the absence of noise) exactly determines the tilt parameters of the aberration. A slightly modified set of Zernicke polynomials may be constructed such that only the tilt terms move the c.g.

Previous work has shown the c.g. to be rather sensitive to quantization noise (and presumably any other sort of noise) on the PSF. In the work reported here, we have assumed that the tilt problem will be dealt with in some appropriate fashion. The aberrations tested had no tilt errors.

Five more moments around the c.g. were defined; the weighting factors were taken to be the aberration polynomials themselves. They are:

$$M_1 = \int (x'^2 + y'^2) P dxdy/E$$
 $M_2 = \int x' y' P dxdy/E$
 $M_3 = \int (x'^2 - y'^2) P dxdy/E$
 $M_4 = \int x' r^2 P dxdy/E$
 $M_5 = \int y' r^2 P dxdy/E$,

where $x' = x - x_{cg}$
 $y' = y - y_{cg}$

Some intuitive meanings may be assigned to these moments. M_1 is an indication of the overall width of the PSF. M_2 is large and positive for a PSF of an elliptical sort of shape, with the long axis oriented at 45° to the X axis. It is negative for the long axis along 135°. The greater the asymmetry between the long and short axes, the larger the magnitude of M_2 . M_3 is similar to M_2 except that the orientations for maximum magnitude are 0° and 90°. Orientations of the long axis at other angles give contributions to both M_2 and M_3 . M_4 and M_5 measure the asymmetry along either the X or Y directions relative to the c.g. A PSF like Figure 13 would have a positive M_4 value.

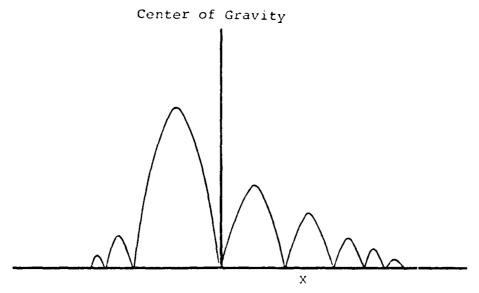


Figure 13 PSF with large positive M_A

Sofware was written to calculate these moments from similated PSF's. An investigation was made of the sensitivity of the moments to noise on the PSF. Table 6a shows the five moments and the c.g. for the PSF from an aberration consisting of 1/4 wave of 45° astigmatism and 1/4 wave of x-coma. The sample spacing of the PSF is $\lambda F\#/2$. The first line shows results with no no 3e. The next two lines show the averages and standard deviations of the moments for 100 realizations of signal-independent white noise on the PSF. The noise variance was 1.85% of the maximum value of the diffraction-limited PSF. Since this aberration has a Strehl ratio of .468, the variance was 3.95% of the peak value of the aberrated PSF. The variation of the moments is too large for them to be useful. Figures 14 and 15 show this PSF noise-free and with noise.

Table 6

Moments and Centers of Gravity

~
ج,
3
ō
C
-
3
\sim
8
z
πt
6 a
w

Y c.g.	16.97017 16.84488 1.18405	
x c.g.	17.83975 17.80108 1.17613	
M.	-9.06288 -17.61442 307.76523	
Æ 4	17.68840 40.25219 359.42038	
M 3	2.54868 0.34411 12.84923	
M ₂	-0.02660 0.70817 12.31852	
M	18.43915 11.16394 26.04207	
	Noise-free Average Standurd Deviation	

ent Calculations

		6b Gaus	6b Gaussian Window on Moment Calculations	on Moment	arcatacions		
3	5 56922	-0.01721	1.23211	1.58887	0.21246	17.83975	16.97017
NOISCILLE		0 1 2020	0.96507	-0.63317	0.46233	17,80108	16.84488
Average	1.39//6	0.555		73030 01	12 05371	1,17613	1.18405
Standard	2,42691	1.27252	1.68210	13.23904	1 7 7 7 7 7 7 7 7 7 7 7 7 7 7 7 7 7 7 7		
Deviation							

Gaussian Window on Moments and Center of Gravity 29

,		0.00154	1.03292	4.87469	0.3419	17,41641	16.99483
Noise-free	5.184/3	10000		0 (03/ /	-0.28306	17.44165	16.96510
Average	5.32479	0.05235	1.00183	0 10 n		00000	0 29117
Standard	0.62237	0.29024	0.39897	2.71539	2.02424	0.32330	•
Daviation							

0	0	0	0	0	0	0	0	0	0	0	•	0	0	0	0		0	•	-	0	0	•	9	0	0	0	0	0	9 0	•
0	•	0	၁	0	0	•	0	0	0	0	0	0	0	0	0	0	0	0	0	0	0	0		0	0	0	-	- 1	0	•
၁	9	0	3	-	0	0	0	0	0	=	>	3	0	0	0	0	-	-	0	0	0	0	•	0	•	0	0	-	00	•
0	0	0	0	٥	c	0	•	0	0	0	-	-	0	0	0	0	0	0	0	0	0	-		0	0	0	0	0	• •	•
c	-	0	٥	٥	0	0	0	c	c	0	c	Þ	0	-	0		-	-	-	-	0	0	-	0	0	0	0		0 0	-
3	-	0	0	þ	0	=	c	э	c	0	0	0	9	>	0	0	0	0	c	0	0	_	-	0	0	-	0	0	9 0	-
9	0	0	2	3	0	9	0	-	0	-	-	9	0	-	-	-			_	-	0	0	-	-	3	_	-	•	0 0	• •
0	•	0	0	0	c	0	0	0	0	0	0	0	-	0	0	•	0	0	0	0	~	~	0	0	-	0	0	0	۰.	• •
0	-	0	0	0	0	0	0	0	0	0	0	0	0	_	-	-	7	~	~	7	-	~	~		-	7	2	0	ə c	•
0	0	9	_	0	-	0	0	_	9	0	0		-		c	9	5	0	0	~	•	~		~	-	~	-	-	- <	-
9	0	9	0	c		9	0	0	0	0	0	-	Þ	~	~	2	~	9	10	s	9	10	~	~	~	0	-	0	- :	-
0	0	0	0	0	0	c	c	0	0	0	-	c	7	•	4	m	~	~	#	23	•	^	-	-	~	0	-	_	00	•
0	0	_	0	٥	0	0	0	∍	0	٥	0	0	-	•	4	4	35	54	24	56	24	~	1	~	~	~	-	7	o -	• 0
_	. 0	-	0	0	0	c	0	_	0	-	-	~	S	28	47	61	7.4	52	0.8	0	55	9	4	4	-	~	Þ	-	٠.	• 0
-																		_											٠.	
																														- 0
																														- 0
															• •															-0
																		_												- 0
•	•	٥ د	•	: 2	· c	: 0		. =	9	0	-	c	~	4	4	~	-	7	ž	27	1	7	٢	-	~	c	-	-	٥ (- 0
c	• •	· c	• •	ء د	. –	. 0	0	0	0	0	0	-	c	~	~	~	~	£	0.0	٨	£	10	7	~	~	٥	-	0	- •	-
_	o c	> =	-	٠.		• 5	0	-		0	0	-	-	-	0	ت	0	0	٥	m	¢	•	-	~	-	~	-	-	- (= -
٥		• •	> =	: =		, 5	0	, 5	9	0	9	٥		-	-	-	~	~	~	.~	-	7	~	-	_	~	>	0	٥ (5 c
=	•	> =	> :	, :	0	, 0		• =	· >	0	ء د	0	-		0	Э	=	=	٦)	^	~	0	0	-	9	3	3	٠.	- 0
c	> =	> =	• =	•	0	ی د			. >	-		0	c	_	-	-	-	-	,	-	>	9	-	-	0	-	-	0	o ·	0
•	۰ -	٠ ،	• •	•	> =	÷ c	•	• =	, ,	0	, 5		0			0	· >	• •	9	3	=	-	-	0	3	-	•	c	0	o
<	: -	• :	•	. :	· c		7	, =	, =	9	, =			-	• >		-	_		-)	0	-	þ	0	0	0	_	9	o =
3	> =	> :	> 5	> =	· -	> =		: 2	0		-	. ~	0	- =	0	0	5	0	٥	6	э	-	-	>	0	2	3		0	0 0
:	: :	•	•	· •	• =	o c	: 0	: 2		ت	· c	~	c) =	. 5	: -	_	-	ت	ς.	5	o	0	0	9	0	c	-	>	00
5	> a	o 1	5 6	: 4	.	: 0	> <	: 3) c	0 0	, =	: 0	3		, 3			3	, =	, 0	c	-	9	· c	=	-		>	00
:	> :	.	,	•	•	> =	ى د	> =	> -	, ,	• =		· =		- =	-	. 3	٥	-		-	0	0	၁	9	2			9	9 3
;	.	> :	: :		2 2			- =	; =		• =	. =	: 3	. 3		. =	: ::			. =	=	ے		_					c	၁၁

Figure 14 Aberrated PSF, Nyquist sampling

200044-4414-1040-1442-00-11-0-2 2362424642444888462244633-23-23/20 1777204477222772644867247777777

igure 15 Aberrated PSF with noise, Nyguist sampling

To reduce the effects of noise, a Gaussian window was applied to the moment calculations, as in

$$E = \int e^{-(x^2+y^2)/w^2} P dxdy/E$$

$$M_1 = \int (x^2+y^2) e^{-(x^2+y^2)/w^2} P dxdy/E$$

The width w was taken to be 5 sample spaces. This eliminates the contribution from small noise fluctuations located at large distances from the c.g., which weight heavily into the moments. This significantly reduced the variations, but they are still too large, as shown in Table 6b.

The successful strategy was to also apply the same Gaussian window to the c.g. calculation. The c.g. was first computed as before, and then recomputed with the Gaussian window centered on the first c.g. estimate. As may be seen in Table 6c. the standard deviation of the c.g., and consequently the five moments, were reduced by factors of four.

The following procedure was used to test the sensitivity of a search on the moments to noise and aliasing. A table of moments was generated for 1575 PSF's on the grid of five values of each aberration coefficient (-.5, -.25, 0., .25, and .5 waves) for five different coefficients (defocus, 0° astigmatism, 45° astigmatism, x coma, and y coma). (The number of such grid points is reduced from 5⁵ by a factor of nearly one half due to symmetry.) A particular aberration was chosen (.25 defocus, .5 0° astigmatism, -.25 y-coma), which was exactly one of the grid points. Moments were calculated from the corresponding PSF's for various amounts of noise and aliasing. The table of moments was searched for the best fit to the moments from the noisy PSF's. In the absence of noise, the moments in the table corresponding to the same aberration as the test case would be a perfect match. With enough noise, some other aberrations will have better fits to the trial moments.

At each noise level, one hundred different noise realizations on the PSF were run through the moment calculation and search. Counts were made of the number of cases in which more than a certain number of aberrations had better fits to the noisy trial moments than the moments corresponding to the actual aberration. The worst case (with the largest number better than the actual aberration) was also noted. The worst case indicates how deep in the list of best fits to the moments a search over the PSF itself must go, to insure inclusion of the correct PSF in the PSF's examined. Table 7 presents the results, in terms of the rank of the correct grid point (correct phase).

From Table 7 we see that, for example, with a detector size equal to the Nyquist sampling interval (1 x 1 case) and with 50% dependent noise, there were 13 noisy PSF's (out of 100 tested) where the correct phase was not ranked number 1. The worst rank was number 10.

The noise was added to each point of the PSF by

$$PSF(X,Y) = PSF(X,Y) (1 + N1 · AD) + N2 · AI$$

where N_1 and N_2 are independent random variables with zero mean and a variance of one. A_D and A_I are the amplitudes of the dependent and independent noise terms. The independent noise amplitude is given as an absolute number and as a percentage of the peak value of a diffraction-limited PSF and of the peak value of the aberrated PSF.

In the case of no aliasing, a remarkable amount of signal dependent noise can be tolerated. Even with $A_{\rm D}$ equal to 70%, the worst case had only 28 grid points with a better fit to the moments. The permissible dependent noise drops roughly with the linear amount of aliasing. The number of PSF data points drops with the square of the aliasing factor. The permissible signal independent noise expressed as a percentage of the peak value of the aberrated PSF also drops in a linear manner, but a much smaller amount of noise can be tolerated.

Table 7
Cumulative Histogram of the Rank of the Correct Grid Point

For each noise level 100 noisy PSF's are subjected to the grid search.

K = Index of the Kth noisy PSF, K = 1,2, . . ., 100,

 X_{K} = Rank of the correct grid point out of all 1575 points tested in the K^{th} search.

Detector		Noise Level	Num	ber o	f time	2S	Largest		
Size (units of	Independent		Dependent	X _K i	, X				
λF#/2)	% of D.L. peak	% of signal peak	of the noise- less signal	1 6		11	101		
lxl	.92	6.6		14	5	1	0	17	
	1.39	10.0		42	19	13	1	149	
	1.85	13.2		53	26	22	2	672	
			10	0	0	0	0	1	
			20	0	0	0	0	1	
			40	9	0	0	0	3	
			50	13	2	0	0	10	
			60	30	9	2	0	16	
			70	38	14	6	0	29	
2×2	.8	4.4		28	14	7	0	15	
			30	34	10	7	0	39	
·····		!	50	59	27	15	4	207	
4×4	.45	1.8		8	0	0	0	3	
	.90	3.7		31	7	1	0	17	
	1.8	7.3		83	55	41	4	226	
			5	0	0	0	0	1	
			10	13	1	0	0	7	
		<u> </u>	20	52	19	13	1	116	
5x5	.44	1.4		1	0	0	0	2	
	.89	2.3		17	7	6	0	67	
	1.78	5.5		67	44	30	10	920	
		i	10	6	0	0	0	5	
	1		15	2.3	10	4	1	132	

6 PHASE DIVERSITY IMAGING

In the previous contract we developed several algorithms to perform phase retrieval on distorted images of extended objects. The optical system introduces a phase aberration $\theta(f)$ with its corresponding PSF p(x). The observed image is

$$z(x) = o(x) * p(x) + n(x),$$

where "*" means convolution, o(x) is the unknown, extended object and n(x) is noise.

Since o(x) is unknown, we cannot use the algorithm of Section 2 to find $\theta(f)$. However, phase retrieval is still possible if we can acquire two images $z_1(x)$ and $z_2(x)$ of the object. These two images allow us to make a joint estimate of o(x) and $\theta(f)$. The details are in the previous Final Report (Appendix C). Briefly, for an estimated object $\hat{o}(x)$ and estimated PSF's $\hat{p}_1(x)$ and $\hat{p}_2(x)$, we calculate an error metric

$$E = \int [z_1(x) - \hat{o}(x) * \hat{p}_1(x)]^2 dx$$
$$\int [z_2(x) - \hat{o}(x) * \hat{p}_2(x)]^2 dx.$$

When we use Parseval's theorem to perform this calculation in the spatial frequency domain, we can minimize E by choice of $\hat{O}(f)$: namely

$$\hat{0}(f) = \frac{\hat{P}_{1}^{*}(f)Z_{1}(f) + \hat{P}_{2}^{*}(f)Z_{2}(f)}{|\hat{P}_{1}(f)|^{2} + |\hat{P}_{2}(f)|^{2}}$$

We substitute this $\hat{0}(f)$ into the E-metric calculation and find the $\hat{\theta}(f)$ that further minimizes the integrals. The θ -search is now identical to that of Section 2.

To implement this algorithm we have chosen to add a known phase $\phi(f)$ to the already phase-aberrated optical system. With $\phi(f) = 0$ we obtain the first image $z_1(x)$; with $\phi(f) \neq 0$ we

get $z_2(x)$. In practice $\phi(f)$ is quadratic so that $z_2(x)$ is an intentionally defocused version of $z_1(x)$. We call $\phi(f)$ a phase diversity and the technique phase diversity imaging.

The algorithm is shown in block diagram form in Figure 16.

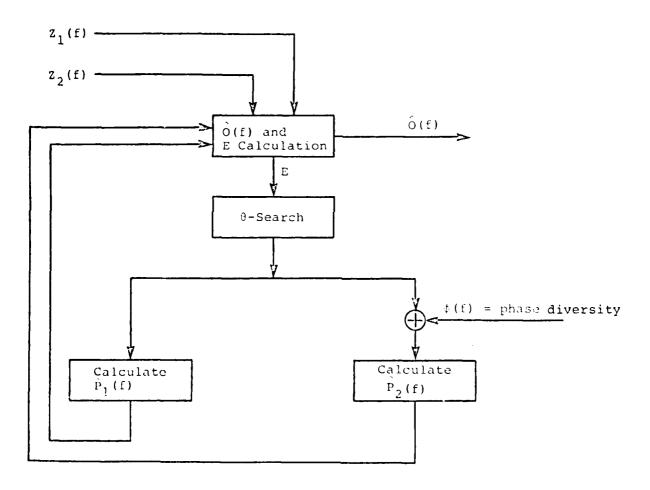
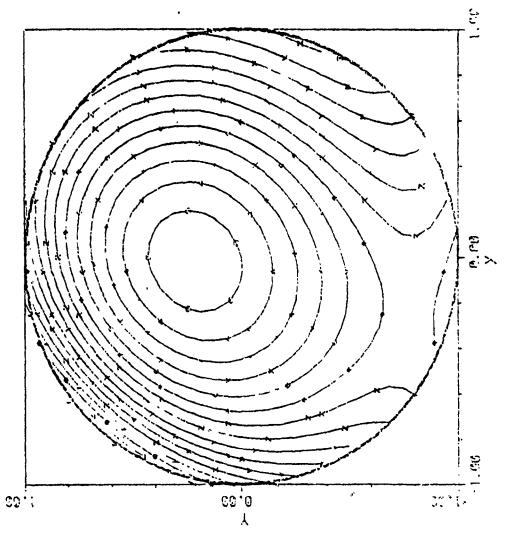


Figure 16 Estimation of 9(f) and the Object Spectrum

Now we show a computer simulation of the technique. A point is imaged through an aberrated optical system, with and without an intentional defocus. The two point spread functions are measured and are used to estimate the object. The estimation procedure, of course, has no knowledge about the object.

In Figure 17 we show a two-dimensional phase aberration θ in a circular, unapodized aperture. The resulting point spread function of the optical system is shown in Figure 18. Next, we intentionally defocus the system (one-half a wave of quadratic phase from the center to the edge of the aperture). The new phase $(\theta + \phi)$ is shown in Figure 19 and the corresponding point spread function in 20.

In this example we add no noise so that z_1 and z_2 , the observed signals, are those shown in Figures 18 and 20. Their Fourier transforms, z_1 and z_2 , are the inputs to the block diagram of Figure 16. The outputs are $\hat{\theta}$ (an estimate of θ) and $\hat{0}$ (an estimate of the object's spectrum). The former is shown in Figure 21 and should be compared with Figure 18. The agreement is excellent. The inverse Fourier transform of $\hat{0}$ is the estimated object. This is shown in Figure 22.



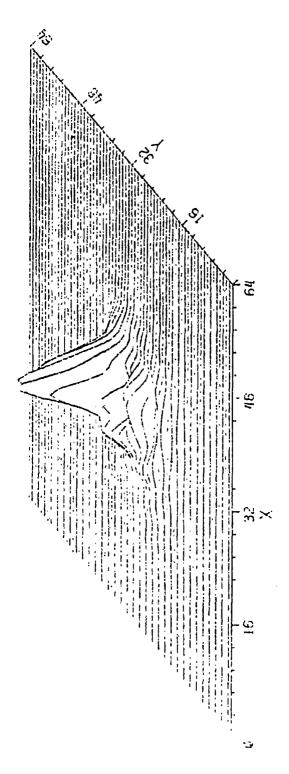
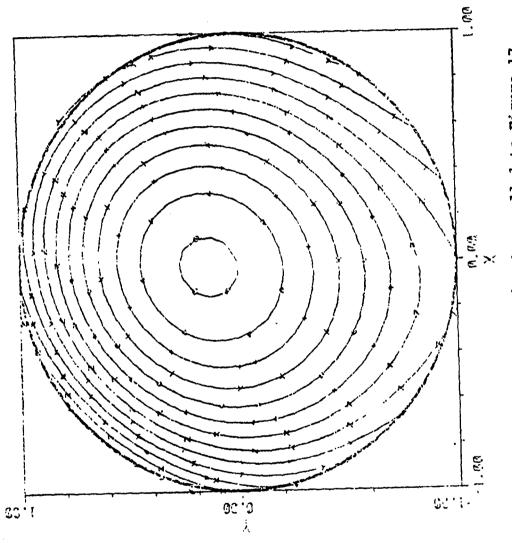


Figure 18. Observed point spread function corresponding to Figure 17

6 6.000 7 100 8 300 9 300 9 300 7 500 7 600 7 800 7 900 8 1.000 1.100



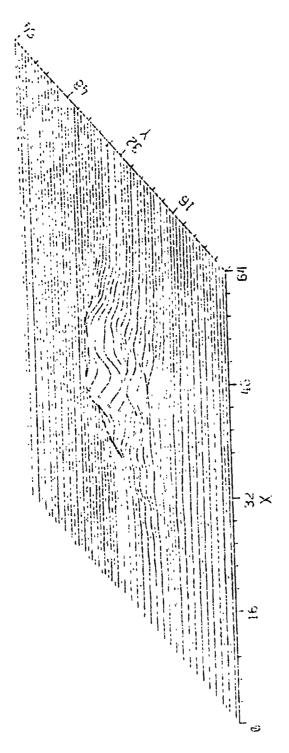


Figure 20. Observed point spread function (defocused version of Figure 18)

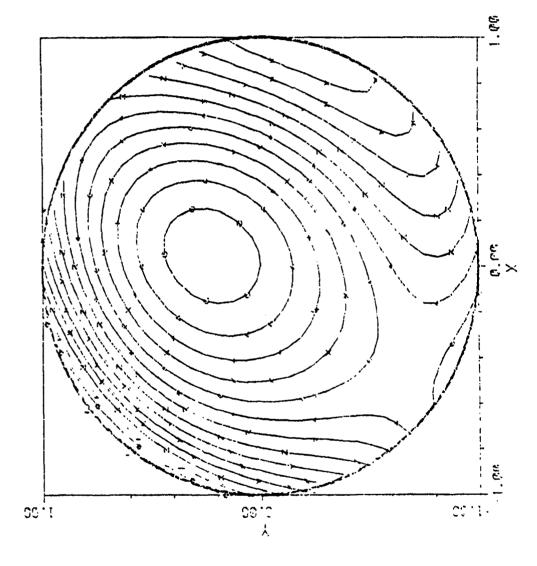
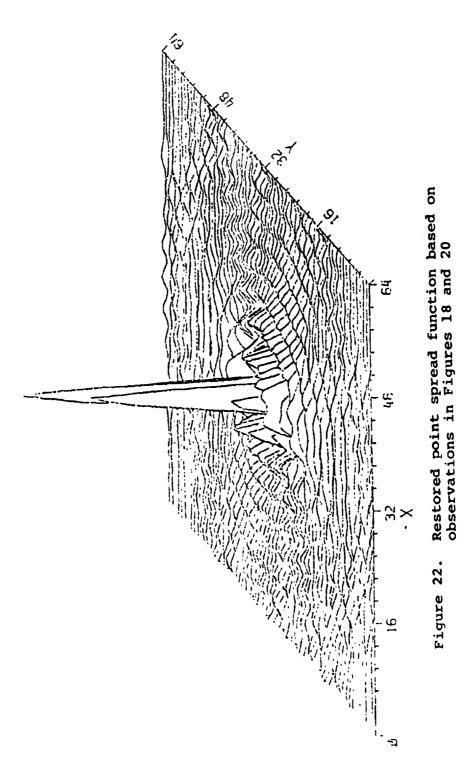


Figure 21. Phase retrieval estimate of Figure 17 based on Figures 18 and 20



Next we present a computer simulation where the object is a segment of a water tower as shown in Figure 23(a). The initial system aberration is the same 0 as in Figure 17. The resulting image is shown in Figure 23(b) and the defocused image is shown in Figure 23(c). The Fourier transforms of the images in 23(b) and 23(c) are the inputs to the algorithms of Figure 16. The result is shown in Figure 23(d).

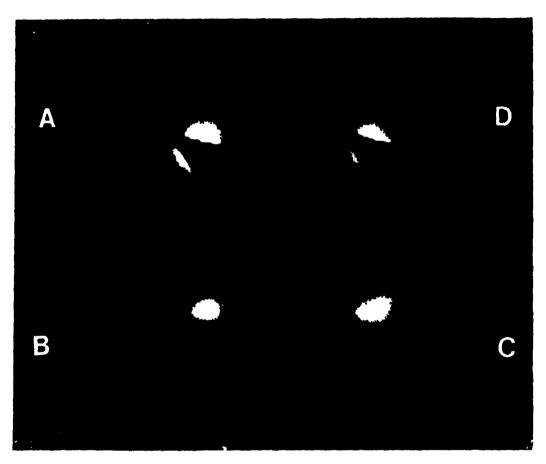


Figure 23. (a) Original, diffraction-limited in me-

- (b) Abore at lineage
- (a) Aborrated and desocused image
- (a) Department among other (b) and (c) compared to the acceptate at impter the phase about at one and the boat some and

When the phase diversity is quadratic, successive images represent the images taken at different values of defocus. This is common practice in electron microscopy for reconstruction of the phase of an object under observation. It seems reasonable to expect that a particular kind of phase diversity, other than quadratic, will allow better object reconstruction for particular kinds of channel distortions.

The main utility of the technique may be the fact that the adaptation is not done in closed loop fashion. Thus, the adaptive optics does not have to track the temporal variation in the channel. The phase diversity allows the images to be unscrambled in post-processing. On the other hand, it would probably be advantageous to include a closed loop with a long time constant to remove gross distortions in the channel. This concept could greatly reduce the burden on the adaptive control mechanism while increasing the burden on post-processing hardware.

7 LABORATORY EXPERIMENT

7.1 Laboratory Set-Up

A procedure has been developed to experimentally test the phase retrieval concept for extended objects. This procedure is similar to earlier experiments in which image data from an optical system is recorded. The optical system contains a known phase aberration function. This function is contained on a clear substrate and is separable from the rest of the optical system. Analysis of the aberration alone is possible by interferometric techniques. This result provides the knowledge of the function against which the retrieved phase is to be compared. To supply sufficient data for phase retrieval of the aberration function in this experiment, the image is recorded at two positions of known focus difference.

The imaging system is sketched in Figure 24. It is a 1:1 projector with condenser illumination. The lamp illuminates a ground glass diffuser. The diffused lamp image is relayed by the condenser to the system aperture stop. At the condenser are filters to limit the spectral transmittance of the system to red light. The aperture stop is located midway between two acromats. Each acromat is 260mm in focal length. A 1:1 objective is made by placing the object and image conjugate at the focus of each lens. The region between lenses contains collimated rays. It is in this region that the phase aberration is inserted. The effect of the aberration on the optical system is therefore the same as its effect in the collimated beam of an interferometer. This maximizes the agreement between the interferometric measure of the aberration and that found by phase retrieval.

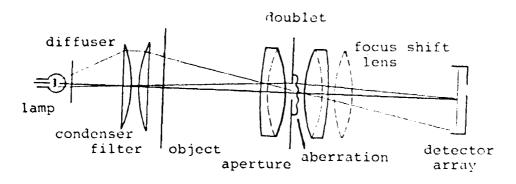


Figure 24. Imaging system

The second doublet focuses the image onto a plane which is scanned by a photodiode array. The array has 1024 elements with 15 μ m center to center spacing. The array is stopped 15 μ m at a time to produce a sampled image of 1024x1024 pixels.

The phase aberration can be inserted or removed repeatably between the doublets. A singlet of 1000mm focal length can also be inserted behind the second lens. This lens controllably defocuses the image.

The spectral distribution of the illumination was chosen to be primarily red, the region of peak diode sensitivity. It was desired to be a broad bandwidth for incoherent imaging yet narrow enough to use its central wavelength for calculations which are wavelength dependent. The relative spectral response of the system is centered at 640nm with a spread, roughly, of 100nm. It is the combination of the lamp distribution at 2850K, an infrared sharp cutoff filter, a red broadband interference filter and the spectral response of the photodiodes.

The aperture size of 2.2mm and focal distance of 260mm gives an F# of ll8. This was selected to give a diffraction limited spread function width of 10 diodes (150 μ m), a suitable sampling density for the phase retrieval algorithm.

A two beam interferometer was constructed to provide a direct measure of the aberrations used. The setup was standard. One beam of parallel wavefronts is the reference and the other is the signal beam. The aberration is placed in the signal beam and the two beams, when recombined, display an interference pattern. This pattern is recorded on film as an interferogram. An example is shown in Figure 25. This aberration appears to have about two waves of distortion and was used to produce the images shown later.

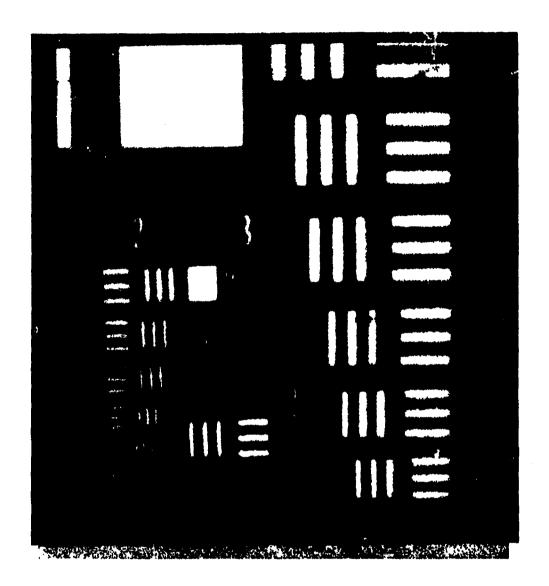


Figure 25. Phase aberration interferogram

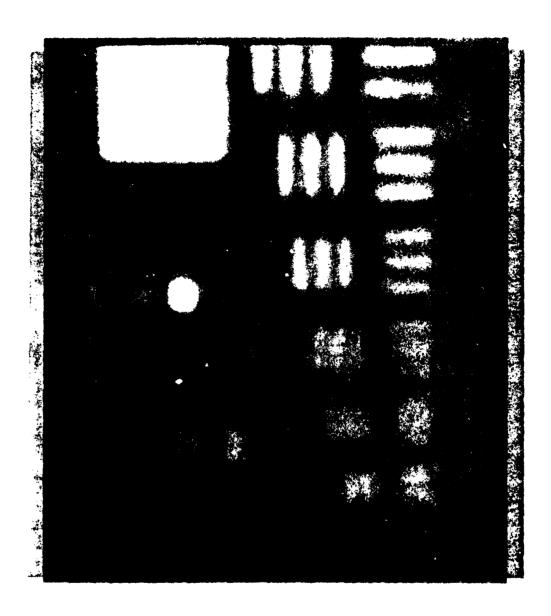
7.2 Data

Figures 26-29 show a series of images. These represent the four imaging conditions which were available in this experiment. Figure 26 shows an image of a section of a tri-bar target produced by the diffraction limited system. Figure 27 shows the same image with +0.9 waves of defocus added by including the defocusing lens in the system. Figure 28 shows the system with the aberration of Figure 25 added at the aperture stop. Figure 29 shows the effect of the same aberration and +0.9 waves of defocus.

In later data processing we used images in Figures 28 and 29 to determine, by our two-focal-plane algorithm, the wavefront distortion.



of sure 25. On the contract the



Entre:

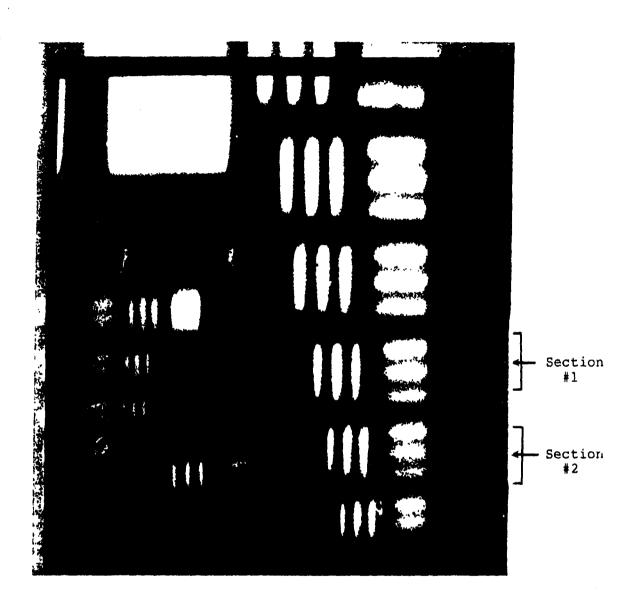


Figure 28. Aburrated image

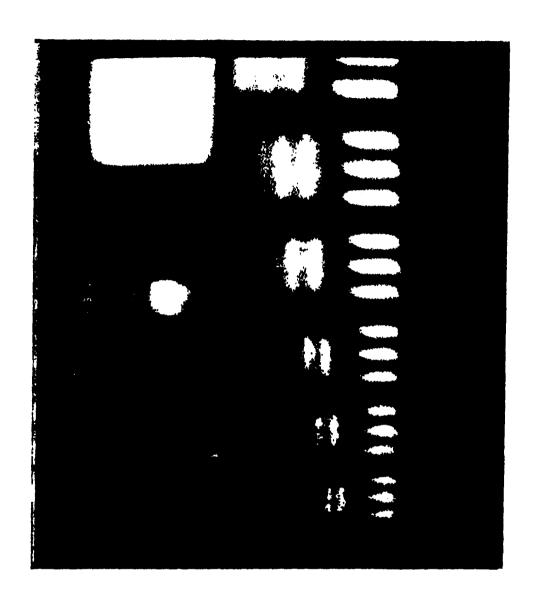


Figure 29. Aberrated and detocused image.

7.3 Determination of the Quadratic Phase

Two measured diffraction limited images (one with quadratic phase added to the phase and one without) were input to the phase-retrieval algorithm. The images used are given in the preceding section (Figures 26 and 27). The idea was to determine, from these two images, the estimated phase distortion across the aperture of the system. By imposing the known focus error between the two images, the calculated phase-estimate should be a constant and thus verify that the estimated focus error is correct. The first step in processing the data was to obtain a smaller region of the images to use as input to the algorithm, for the simple reason that the entire image would have been burdensome computationally. Corresponding 80x80 pixel regions of each image were chosen for processing. The actual region corresponds to the area surrounding the number "4" in the right side of the tri-bar target in Figure 26.

The first moment (center of gravity) of each image was calculated so that each image could be aligned to remove major tilts in the phase estimate. The slow Fourier transform was performed on each section, each output transform being a 17x17 sampled OTF. The transform was sampled so that the outer point corresponds to the diffraction-limited cutoff of the system. These two OTF's were then input to the two-focal plane phase-retrieval search algorithm in order to estimate the phase. The input focus error was assumed to be 0.9 waves.

The phase estimate found from the search algorithm is given in Figure 30. The RMS phase was calculated to be .022 waves and is .06 waves peak to peak. The result is consistent with a diffraction-limited phase to within the errors expected in the experimental procedure.

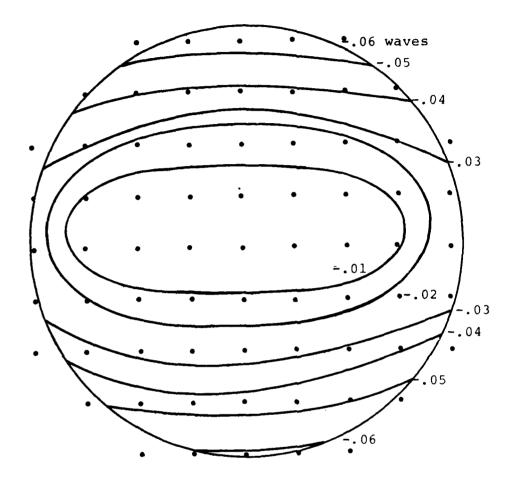


Figure 30. Diffraction limited phase estimate

7.4 Determination of the Unknown Aberration

The two aberrated images (one with focus error added and one without) were input to the phase retrieval algorithm. The same corresponding 80x80 images section used for the diffraction limited (Number "4") was processed using the exact same procedure as the diffraction limited case. The phase retrieval algorithm was allowed to search over 20 Zernike coefficients in order to fit the correct phase. The Zernike coefficients are given in Figure 31 and a contour plot of the phase is given in Figure 32. The actual phase aberration that was measured interferometrically is given in Figure 33.

Pl = 0.	P11 = .03
P2 = .10	P12 = .02
P3 = .17	P13 = .009
P4 =07	P14 =048
P5 =26	P15 = .0
P6 =21	P16 = .22
P7 = .03	P17 = .12
P8 = .006	P18 =05
P9 =063	P19 = 0.
P10 = .07	P20 = 0.

Figure 3.1 Zernike polynomial coefficients obtained from phase retrieval algorithm - applied to two-focus problem (aberrated case)

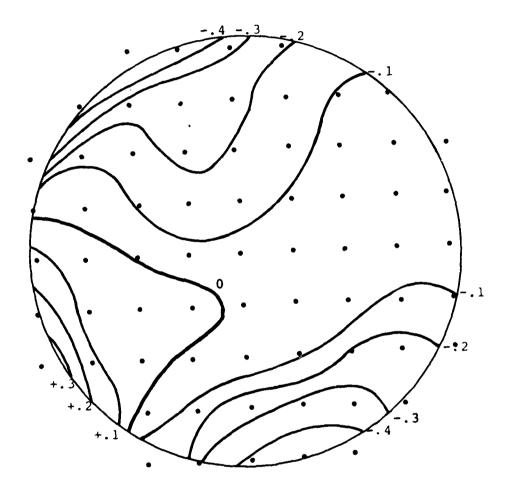


Figure 32. Estimated phase from phase retrieval algorithm applied to aberrated data

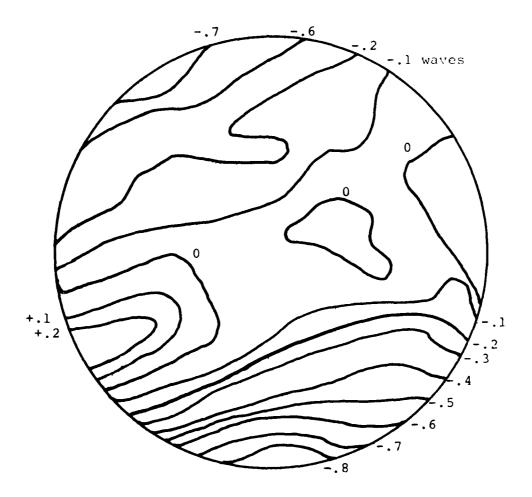


Figure 3.3. Measured phase from interferogram

8 BLIND TEST

To test the phase retrieval algorithm, the customer requested that personnel from Draper Lab give us several noisy, undersampled point spread functions. These were prepared by Dr. V.N. Mahajan and his staff at the Optical Systems Division in Cambridge, MA. We subsequently received three aberrated point spread functions, each "sampled by an 8×8 array of detector elements. The width of the detector elements is $2.13\lambda F$, where λ is the wavelength of the object radiation and F is the focal ratio (f#) of the optical system."* The three point spread functions are shown in Figure 34.

Figure 34. PSF's for the blind test

(c)

Letter of June 30, 1981 to R. Gonsalves from V. Mahajan

We exerc'sed the phase retrieval algorithm on the three point spread functions (PSF) as follows. First, we left the sampling interval at 2.13 λ F#, even though our algorithm assumes the prefix constant to be a integer (we used 2). For each PSF we assumed hat the unknown phase could be approximated by 8, by 15, and by 23 terms in a Zernike polynomial expansion. The 8 and 15 term expansions were determined with the all-zero polynomial as a starting point in our search. The 23 term expansion used the 8 term solution as a starting point.

Next we interpolated the PSF's to give us an 8x8 array sampled at $2\lambda F\#$. The searches described above were repeated.

In Figure 35 we list the Zernike polynomials.

Figure 36 is a summary of the data processing for the 18 cases.

Figures 37 through 82 give the results. For example, Figure 37 shows the input PSF, the estimated PSF, the mean square error between them, and the coefficients of the Zernike polynomials for the estimated phase. Figure 38 shows the estimated phase itself. This first pair of figures is for case 1, sampling interval = $2.13\lambda F\#$, and 23 Zernike polynomials.

n	Rectangular Coordinates	Polar Coordinates
1	1	1
2	×	cus 0
3	y	sin 0
4	$2x^2 + 2y^2 - 1$	$2r^2 - 1$
5	x ² - y ²	r ² cos 2 8
6	2 xy	r ² sin 2 θ
7	$\times (3x^2 + 3y^2 - 2)$	$(3r^2-2r)\cos\theta$
8	$y(3x^2+3y^2-2)$	$(3r^2-2r) \sin \theta$
9	$x(x^2-3y^2)$	r ³ cos 3 6
10	$y(3x^2-y^2)$	r ³ sin 3 0
11	$6x^4 + 12x^2y^2 + 6y^4 - 6x^2 - 6y^2 + 1$	$6r^4 - 6r^2 + 1$
12	(x^2-y^2) $(4x^2+4y^2-3)$	$(4r^4-3r^2)$ cos 2 8
13	$2xy (4x^2 + 4y^2 - 3)$	$(4r^4-3r^2)$ sin 2 θ
14	$x^4 - 6x^2y^2 + y^4$	r ⁴ cos 4 θ
15	$4xy (x^2-y^2)$	r ⁴ sin 4 θ
16	$\times (10x^4 + 20x^2y^2 + 10y^4 - 12x^2 - 12y^2 + 3)$	$(10r^5-12r^3+3r)\cos\theta$
17	$y(10x^4+20x^2y^2+10y^4-12x^2-12y^2+3)$	$(10r^5-12r^3+3r) \sin \theta$
18	$x(x^2+y^2)(5x^2+5y^2-4)$	$(5r^5-4r^3)$ cos 3 θ
19	$y(x^2+y^2)(5x^2+5y^2-4)$	$(5r^5-4r^3)$ sin 3 θ
20	$x^5 - 10x^3y^2 + 5xy^4$	r^5 cos 5 θ
21	$5x^4y - 10x^2y^3 + y^5$	r^5 sin 5 θ
22	$20x^{6} + 60x^{4}y^{2} + 60x^{2}y^{4} + 20y^{6} - 30x^{4} - 60x^{2}y^{2}$ $- 30y^{4} + 12x^{2} + 12y^{2} - 1$	$20r^6 - 30r^4 + 12r^2 - 1$
23	$70x^8 + 280x^6y^2 + 420x^4y^4 + 280x^2y^6 + 70y^8$	$70r^8 - 140r^6 + 90r^4$
	$-140x^6 - 420x^4y^2 - 420x^2y^4 - 140y^6 + 90x^4$	$-20r^2 + 1$
	$+ 180x^2y^2 + 90y^4 - 20x^2 - 20y^2 + 1$	

Figure 35. Zernike circle polynomials

Assumed Sampling Interval	Case	Number of Zernike Polynomials	Residual Mean Square Error	RMS Value of the Estimated Phase (in waves)
	1	23 15 8	14669 16113 18750	0.368 0.327 0.419
2.13λF#	2	23 15 8	14792 14977 17158	0.187 0.215 0.197
	3	23 15 8	113471 114310 114005	0.434 0.341 0.431
	1	23 15 8	10980 12927 15518	0.451 0.362 0.486
2.00\F#	2	23 15 8	9870 10553 14042	0.213 0.224 0.231
	3	23 15 8	143020 143689 143503	0.541 0.506 0.536

Figure 36. Data Processing Summary

PHRUN25.LOG:1

24-JUL-1981 16:40:13.60

NUMBER OF ZERNIKE POLYNOMIALS = 23 NUMBER OF ITERATIONS = 100 ACTUAL NUMBER OF ITERATIONS = 29

			INP	T P	SF					ESTI	MATE	ED PS	F		
-18	- 9	-5	-11	33	13	-7	-15	0	0	1	3	4	0	0	0
6	1	27	33	30	4	- 3	0	0	0	0	9	21	2	0	0
-45	-15	2	29	179	12	27	0	1	1	2	22	169	11	1	1
14	-3	6	66	352	58	-15	-4	1	1	2	57	343	49	1	1
- 2	12	1	61	95	58	-11	3	0	0	2	50	86	47	2	0
29	-20	3	16	34	13	5	15	0	0	1	9	12	4	2	n
-2	- R	26	35	11	- 4	-19	-14	0	0	1	5	2	0	0	1
-16	- A	-12	-8	-15	-30	~6	-25	0	0	1	2	1	0	0	0

MEAN SQUARE ERROR = 14669.0371

COEFFICIENTS OF THE ZERNIKE POLYNOMIALS

K	P(K)		
t	0.20000		
2	-0.51416		
2 3 4	0.32499		
4	0.03853		•
5	0.37366		
6	-0.18525		
6 7	-0.18813		
8	-0.05068		
9	0.01493		
10	0.00606		
1 1	0.04404		
12	-0.05517		
13	-0.18909	Piguro 27	Blind test results for case 1,
14	-0.06202	rigure 37.	
15	-0.11456		2.13 λ F#, 23 polynomials
16	0.06494		
17	0.00804		
18	-0.08093		
19	-0.06974		
20	-0.12625		
21	-0.13419		
22	0.00143		
23	-0.02685		

PHRUN25.LOG;1 24-JUL-1981 16:40:13.60 ESITMATED PHASE ABERRATION (100 = ONE WAVE)

92 99 101 101 100 -10 -5 -5 -4 -2 -20 -19 -18 -15 -11 -6 - 3 **-3**. -37 -36 -33 -27 -19 -13 -2 -4 -7 -2 -6 -10 -10 -56 -54 -48 -39 -28 -18 -9 -2 -6 -10 -10 **-74 -69 -62 -50 -35 -22 -10** -87 -80 -72 -58 -42 -25 -11 -3 -5 -4 -82 -75 -63 -46 -29 -13 -72 -67 -59 -46 -31 -17 -4 -46 -43 -38 -30 -20 -12 -6 -2 -17 -21 -22 -22 -20 -19 -18 -17 -15 -11 -12 -23 -31 -38 -44 -48

RMS PHASE ACROSS APERTURE = 0.368 (WAVES)

Figure 38. Blind test results for case 1, $2.13\lambda F\#$, 23 polynomials

PHRUN25.60G; 1

27-JUL-1981 15:16:36.82

NUMBER OF ZERNIKE POLYNOMIALS = 15 NUMBER OF ITERATIONS = 100 ACTUAL NUMBER OF ITERATIONS = 31

INPUT PSF							E	STI	MATE	D PS	F				
-18	- 9	-5	-11	33	13	-7	-15	0	0	0	1	8	3	0	0
6	1	27	33	30	4	-3	0	0	0	0	5	22	6	1	1
-45	-15	2	29	179	12	27	0	1	0	2	19	168	10	4	1
14	-2	6	66	352	58	-15	-4	0	0	1	63	342	49	5	1
-2	12	1	61	95	58	-11	3	0	1	1	46	91	39	11	1
29	-20	3	16	34	13	5	15	1	0	0	1	2	4	3	3
-2	- 9	26	35	11	-4	-19	-14	0	0	0	0	1	1	0	0
-16	-8	-12	-8	-15	-30	-6	-25	0	0	0	1	3	1	1	0

MEAN SQUARE ERROR = 16113.3584

COEFFICIENTS OF THE ZERNIKE POLYNOMIALS

K	P(K)
1	0.0000
2	-0.52890
3	0.13925
4	0.05675
5	0.08017
6	0.27042
7	-0.18821
8	0.21869
ğ	-0.20175
1 Ó	0.06567
11	-0.05859
1 ?	-0.13863
• •	0.19159
13	-0.07769
14	· · · · · · · · · · · · · · · · · · ·
15	-0.14917

Figure 39. Blind test results for case 1, $2.13\lambda F\#$, 15 polynomials

PHRUN25.LUG:1 27-JUL-1981 15:16:36.82 FSTIMATED PHASE ABERRATION (100 = ONE WAVE)

91 101 108 Н 1) -9 - 3 -5 -5 - 3 -17 -2 -9 -9 -6 -6 -27 -11 -2 -9 -9 -6 -6 -38 -17 В -8 -3 -1 -5 -7 **-** 3 -28 -10 -7 -5 -46 -23 -8 -3 -7 -8 -6 -46 -26 -15 -9 -8 -10 -13 -16 -16 -12 -1 -58 -43 -35 -31 -32 -33 -34 -33 -27 -14

-77 -71 -69 -68 -68 -64

RMS PHASE ACROSS APERTURE = 0.327 (WAVES)

Blind test results for case 1, Figure 40. $2.13\lambda F$ #, 15 polynomials

28-JUL-1981 16:08:13.69

NUMBER OF ZERNIKE POLYNOMIALS = 8 NUMBER OF ITERATIONS = 100 ACTUAL NUMBER OF ITERATIONS = 27

			INP	UT P	SF					ESTI	MATE	ED PS	F		
-18	-9	-5	-11	33	13	-7	-15	0	0	1	5	8	1	0	0
6	1	27	33	30	4	- 3	0	0	0	1	19	39	3	i	0
-45	-16	2	29	179	12	27	0	1	1	1	26	159	11	5	1
14	-2	6	66	352	58	-15	-4	0	1	6	74	348	64	4	1
-2	12	1	61	95	58	-11	3	0	0	0	31	99	5	0	0
29	-20	3	16	34	13	5	15	0	0	0	0	2	0	0	0
-2	- 3	26	35	11	-4	-19	-14	0	0	0	1	1	0	0	0
-16	-8	-12	-8	-15	-30	-6	-25	0	0	0	2	2	1	0	0

MEAN SQUARE ERROR = 18750,3301

COEFFICIENTS OF THE ZERNIKE POLYNOMIALS

K	P(K)
1	0.0000
2	-0.65838
3	0.19238
4	0.09076
5	0.45863
6	0.11742
7	-0.22798
8	0.03849

Figure 41. Blind test results for case 1, $2.13\lambda F\#$, 8 polynomials

PHRUN25.LJG;1 28-JUL-1981 16:08:13.69 ESTIMATED PHASE ABERRATION (100 = DNE WAVE)

134 132 131 131 132 135 98 101 106 -5 Э -23 -15 -38 -28 -20 -13 -8 - 4 -50 -38 -28 -20 -13 **≠** ₽ -1 ŋ - 1 - 3 -7 -62 -48 -36 -26 -17 -11 -6 -1 -1 -9 -12 - 3 **~** 3 -6 -7 -12 -17 -73 -57 -42 -31 -21 -13 -7 -3 -1 -1 -66 -49 -36 -24 -15 -8 -1 -1 -9 -14 -76 -57 -42 -29 -18 -11 -5 -1 -2 -6 -11 -17 -67 -50 -35 -23 -14 -8 -4 -2 -2 -60 -44 -31 -21 -13 -9 -13 -8 -6 . -6

-42 -30 -22 -16 -14 -14

RMS PHASE ACROSS APERTURE = 0.419 (WAVES)

Figure 42. Blind test results for case 1, $2.13\lambda F\#$, 8 polynomials

28-JUL-1981 12:56:30.36

NUMBER OF ZERNIKE POLYNOMIALS = 23 NUMBER OF ITERATIONS = 100 ACTUAL NUMBER OF ITERATIONS = 28

	INPUT PSF								ESTIMATED PSF								
26	-3	5	44	-13	-4	27	-22	0	0	0	1	1	0	0	0		
-22	-33	4	21	11	5	-8	18	0	0	0	1	4	1	0	0		
2	13	-11	-29	56	1 4	6	9	0	0	0	2	50	10	0	0		
-10	3	10	102	240	29	13	1	1	2	13	97	238	24	0	0		
-15	-13	41	209	164	5	-8	21	1	3	30	207	161	15	1	1		
-2	11	16	-6	31	-2	0	16	0	0	2	5	26	3	1	0		
-9	31	2	-12	20	- 3	16	-1	0	0	0	1	2	1	1	1		
-22	24	-8	-17	-21	-16	-25	10	0	0	0	1	1	0	0	0		

MEAN SQUARE ERROR = 14792.0439

K	P(K)			
1	0.00000			
2	-0.12741			
3	-0.15363			
4	-0.01173			
5	-0.19319			
6	-0.04978			
2 3 4 5 6 7 8 9	-0.11550			
8	0.25747			
9	0.02261			
10	0.15956			
11	-0.07124			
12	0.02961			
13	-0.08038			
14	-0.05428			
15	-0.03489			
16	0.06735			
17	-0.15433	77 d mars mars	4.5	D1:
18	-0.04259	rigure	43.	Blind test results for case 2,
19	-0.00326			2.13λF#, 23 polynomials
20	-0.00861			
21	-0.04516			
22	-0.00050			
23	0.00533			

PHRUN25.LOG; 1 28-JUL-1981 12:56:30.36 ESTIMATED PHASE ABERRATION (100 = ONE WAVE) -2 -9 -14 -12 0 -12 -19 -19 -13 - 3 -2 2 -11 -20 -24 -20 -10 - 3 -R -19 -24 -21 -13 - 3 - 4 -4 -15 -20 -19 -12 0 -10 -15 -14 - 3 **-5** - 7 -2 - 3 -1 - 3 -1 -10 -13 -7 ? -1 -21 -22 -17 -11 -8 -6 -5 -29 -30 -27 -23 -20 -17 -15 -11 -7 -39 -39 -37 -34 -31 -27

RMS PHASE ACROSS APERTURE = 0.187 (WAVES)

Figure 44. Blind test results for case 2, $2.13\lambda F\#$, 23 polynomials

NUMBER OF ZERNIKE POLYNOMIALS = 15 NUMBER OF ITERATIONS = 100 ACTUAL NUMBER OF ITERATIONS = 27

			INP	JT P	S F				ESTIMATED PSF								
26	-3	5	44	-13	-4	27	-22	0	0	0	0	0	3	2	0		
-22	-33	4	21	11	5	-8	18	0	0	0	0	4	8	2	1		
2	13	-11	-29	56	14	6	9	0	0	0	2	44	15	1	0		
-10	3	10	102	240	29	13	1	1	3	9	100	236	23	1	1		
-15	-13	41	209	164	5	-8	21	0	2	36	207	160	10	1	1		
-2	11	16	- 6	31	-2	0	16	0	0	1	6	17	5	1	0		
-9	31	2	-12	20	- 3	16	-1	0	0	0	0	1	2	1	1		
-22	24	-8	-17	-21	-16	-25	10	0	0	0	0	0	1	1	0		

MEAN SQUARE ERROR = 14977.6211

K	P(K)
1	0.00000
2	-0.13208
3	-0.18848
4	0.16422
5	-0.14907
6	0.13722
7	-0.10132
8	0.17617
9	0.02508
10	0.24696
11	-0.16436
12	0.06881
13	0.13409
14	-0.00229
15	0.00968

Figure 45. Blind test results for case 2, 2.13λF#, 15 polynomials

PHPUN25.LOG: 1 28-JUL-1981 13:58:32.63 ESTIMATED PHASE ABERRATION (100 = ONE WAVE) -2 -3 -2 -1 -9 -11

RMS PHASE ACROSS APERTURE = 0.215 (WAVES)

Figure 46. Blind test results for case 2, $2.13\lambda F\#$, 15 polynomials

PHRUN25.LOG;1

28-JUL-1981 12:36:51.12

NUMBER OF ZERNIKE POLYNOMIALS = 8 NUMBER OF ITERATIONS = 100 ACTUAL NUMBER OF ITERATIONS = 29

			INP	JT P	SF				ESTIMATED PSF								
26	-3	5	44	-13	-4	27	-22	0	0	0	0	1	1	1	0		
-22	-33	4	21	11	5	-8	18	0	0	0	1	7	5	2	0		
2	13	-11	-29	56	14	6	9	0	0	1	6	59	13	3	1		
-10	3	10	102	240	29	13	1	1	0	2	108	235	27	5	1		
-15	-13	41	209	164	5	~8	21	0	0	1	209	168	24	5	1		
-2	11	16	-6	31	-2	0	16	0	0	0	4	9	3	1	0		
-9	31	2	-12	20	-3	16	-1	0	0	0	0	1	0	0	0		
-22	24	-8	-17	-21	-16	-25	10	0	0	0	0	0	0	0	0		

MEAN SQUARE ERROR = 17158.5293

K	P(K)
1	0.00000
2	-0.20418
3	-0.07825
4	-0.11455
5	-0.24277
6	0.11323
7	-0.09764
8	0.24352

Figure 47. Blind test results for case 2, $2.13\lambda F\#$, 8 polynomials

PHRUN25.L7G;1 28-JUL-1981 12:36:51.12 ESTIMATED PHASE ABERRATION (100 = ONE WAVE)

RMS PHASE ACROSS APERTURE = 0.197 (WAVES)

Figure 48. Blind test results for case 2, $2.13\lambda F\#$, 8 polynomials

28-JUL-1981 15:38:26.96

NUMBER OF ZERNIKE POLYNOMIALS = 23 NUMBER OF ITERATIONS = 100 ACTUAL NUMBER OF ITERATIONS = 21

				ESTIMATED PSF												
-34	-43	14	87	-16	-21	51	108	C)	0	0	1	0	0	0	0
-30	41	22	-9	27	22	43	-7	d)	0	0	2	5	1	0	0
-5	53	-81	-32	166	-27	24	-25	O)	0	0	1	139	2	1	0
53	-63	7	13	375	29	13	40	C		0	1	14	348	20	3	0
57	-2	71	15	122	-2	14	69	C)	0	1	4	95	2	1	1
16	21	-6	-60	56	-41	16	-14	C) 1	0	0	1	11	1	0	0
8	- 37	12	-2	-14	-94	-91	-40		,	0	0	0	1	0	0	0
34	-17	-58	45	-49	-41	-23	-70	C)	0	0	0	0	0	0	0

MEAN SQUARE ERROR = 113471,9531

K P(K)	
1 0.00000	
2 -0.72504	
3 0.33835	
4 0.14078	
5 0.30064	
6 -0.01004	
1	
8 0.02084	
9 0.02034	
10 0.01474	
-0.00880	
12 0.00405	
13 0.01477	
14 0.01639	
15 0.03228	
16 -0.00119	
17 0.00482	
18 -0.01799 Figure 49. Blir	nd test results for case 3,
20 0.04563	3AF#, 23 polynomials
21 -0.01725	
0.00017	
23 -0.00588	

PHRUN25.LOG;1 28-JUL-1981 15:38:26.96 ESTIMATED PHASE ABERRATION (100 = DNE WAVE)

108 111 113 116 119 123 98 103 108 113 116 97 101 104 -17 -3 -23 -11 -4 Ą -28 -19 -14 -9 -6 - 3 -33 -26 -22 -19 -15 -12 -10 -2 -6 -38 -33 -30 -27 -24 -21 -18 -14 -10 -6 -2 -43 -39 -36 -34 -31 -27 -24 -20 -16 -12 -5 -44 -42 -39 -36 -32 -27 -23 -19 -15 -11 -8 -48 -45 -42 -39 -34 -29 -24 -19 -15 -12 -9 -1 -47 -43 -38 -33 -27 -22 -17 -13 -10 -7 -41 -35 -28 -22 -17 -12 -8

RMS PHASE ACROSS APERTURE = 0.434 (WAVES)

-21 -14 -9 -4

-2 -1

Figure 50. Blind test results for case 3, $2.13\lambda F\#$, 23 polynomials

28-JUL-1981 14:12:11.06

NUMBER OF ZERNIKE POLYNOMIALS = 15 NUMBER OF ITERATIONS = 100 ACTUAL NUMBER OF ITERATIONS = 26

			INPL	T PS	F			ESTIMATED PSF								
-34	~43	14	87	-16	-21	51	108	0	0	0	1	4	1	0	0	
-30	41	22	-9	27	22	43	-7	0	0	0	2	14	1	0	0	
-5	53	-81	-32	166	-27	24	-25	0	0	0	2	135	2	0	0	
53	-63	7	13	375	29	13	40	0	0	1	11	351	13	1	0	
57	-2	71	15	122	-2	14	69	D	1	2	8	99	7	2	1	
16	21	- 6	-60	56	-41	16	-14	0	0	0	0	0	0	0	0	
8	-37	12	-2	-14	-94	-91	-40	0	0	0	0	0	0	0	0	
34	-17	-58	45	-49	-41	-23	-70	0	0	0	0	1	0	0	0	

MEAN SQUARE ERROR = 114310.4766

K	P(K)
1	0.00000
2	-0.48972
3	0.37731
4	0.04506
5	0.11653
6	-0.00631
7	-0.19206
8	0.00039
ğ	-0.22465
10	-0.00996
11	-0.03206
12	-0.03229
13	-0.01440
14	-0.06289
15	-0.00741

Figure 51. Blind test results for case 3, $2.13\lambda F\#$, 15 polynomials

28-JUL-1981 14:12:11.06 PHRUN25.LUG; 1 ESTIMATED PHASE ABERRATION (100 = ONE WAVE) 96 100 - 1 -13 -6 -30 -22 -15 -10 -5 -36 -28 -21 -16 -11 **~6** - 2 -39 -31 -24 -19 -14 -10 -1 -5 -40 -32 -26 -20 -16 -11 -7 -2 -39 -32 -26 -21 -16 -12 -7 **-**3 -39 -32 -26 -21 -17 -12 -8 -33 -28 -23 -18 -14 -10 -5 -37 -32 -27 -23 -19 -15 -10 -5 ŋ -41 -37 -33 -29 -25 -20 -15 -10 -5 -52 -49 -45 -42 -37 -33 -28 -22 -17 -11

-71 -67 -64 -59 -54 -49

RMS PHASE ACROSS APERTURE = 0.341 (WAVES)

Figure 62. Blind test results for case 3, $2.13\lambda F\#$, 15 polynomials

28-JUL-1981 15:15:08.26

NUMBER OF ZERNIKE POLYNOMIALS = 8 NUMBER OF ITERATIONS = 100 ACTUAL NUMBER OF ITERATIONS = 22

			INP	JT PS	SF					ESTI	MATE	O PS	F		
-34	-43	14	87	-16	-21	51	108	0	0	0	• 0	1	0	0	0
-30	41	22	-9	27	22	43	-7	0	0	0	1	8	1	0	0
-5	53	-81	-32	166	-27	24	-25	0	0	0	1	140	2	1	0
53	-63	7	13	375	29	13	40	0	0	2	12	350	20	2	0
57	-2	71	15	122	-2	14	69	0	0	0	3	97	3	1	0
16	21	-6	-60	56	-41	16	-14	0	0	0	1	8	1	0	0
8	-37	12	-2	-14	-94	-91	-40	0	0	0	0	1	0	0	0
34	-17	-58	45	-49	-41	-23	-70	0	0	0	0	0	0	0	0

MEAN SQUARE ERROR = 114005.8438

K	P(K)
1	0.00000
2	-0.70795
3	0.35687
4	0.14237
5	0.31047
6	-0.01610
7	0.02125
8	0.01797

Figure 53. Blind test results for case 3, $2.13\lambda F\#$, 8 polynomials

PHRIN25.LUG;: 28-JUL-1981 15:15:08.26 ESTIMATED PHASE ABERRATION (100 = ONE WAVE)

103 109 114 119 124 129

94 99 103 108 112 116 92 97 101 -10 -4 2.2 -22 -15 -10 -4 -32 -26 -20 -15 -10 -5 -1 -10 -34 -29 -24 -19 -14 -10 -6 -2 -47 -41 -36 -31 -26 -22 -17 -13 -9 -6 ~2 б -52 -45 -41 -36 -31 -27 -23 -19 -15 -11 -7 -3 -49 -44 -39 -35 -30 -26 -22 -18 -14 -10 -2 -6 -50 -45 -40 -36 -32 -28 -24 -20 -16 -11 -2 -44 -40 -35 -31 -27 -23 -19 -15 -10 -6 -1

-23 -19 -14 -10 -6 -1

-36 -32 -28 -24 -20 -16 -11 -7 -2

RMS PHASE ACROSS APERTURE = 0.431 (MAVES)

Figure 54. Blind test results for case 3, 2.13λF#, 8 polynomials

28-JUL-1981 16:40:58.35

NUMBER OF ZERNIKE POLYNOMIALS = 23 NUMBER OF ITERATIONS = 100 ACTUAL NUMBER OF ITERATIONS = 25

			INP	UT P	SF				ESTIMATED PSF								
-2	- 2	-6	~ 5	1	-8	0	-2	0	1	3	5	1	0	0	0		
0	5	30	38	32	3	2	4	0	1	5	23	13	5	1	1		
-13	3	-12	41	220	25	15	14	2	1	2	37	207	14	6	3		
-12	11	-1	87	353	80	-29	5	1	3	5	79	345	74	5	1		
4	9	4	65	93	63	- 6	-2	0	0	7	52	89	49	1	0		
2	-23	5	14	31	16	4	17	0	0	1	6	15	11	0	0		
-1	- 7	33	35	20	1	-17	-11	0	0	1	2	4	2	0	0		
-7	-4	-8	0	-19	-31	-8	-28	0	0	1	1	1	0	0	0		

MEAN SQUARE ERROR ≈ 10980.7637

K	P(K)						
1	0.00000						
2	-0.67001						
3	0.36708						
4	0.11526						
5	0.36444						
6	0.04485						
7	-0.04228						
1 2 3 4 5 6 7 8	-0.13217						
	0.05469						
10	0.12285						
11	0.03617						
12	0.04297						
13	-0.16960						
14	-0.07437						
15	0.02564						
16	0.00318						
17	0.04489						
18	0.05263						
19	+u.12719	Figure	55.		test results for	case	l,
20	-0.00918			$2\lambda F#$,	23 polynomials		
21	-0.01912						
22	0.00500						
23	-0.07443		80				

PHPUN25.LOG;1 28~JUL-1981 16:40:58.35 ESTIMATED PHASE ABERRATION (100 = ONE WAVE)

123 120 117 115 113 108 98 101 109 104 -6) -2 -1 -22 -16 -16 -13 -9 -6 -39 -31 -30 -26 -21 -17 -13 -7 -56 -45 -44 -40 -33 -27 -20 -11 θ **-74 -56 -56 -54 -46 -37 -26 -13** - 1 -65 -64 -64 -58 -48 -34 -18 -2 -75 -65 -68 -66 -57 -42 -25 -8 -64 -61 -62 -57 -46 -30 -12 -52 -47 -44 -37 -24 -7

RMS PHASE ACROSS APERTURE = 0.451 (NAVES)

-28 -19 -9

Figure 56. Blind test results for case 1, $2\lambda F\#$, 23 polynomials

PHRUN25.LOG;1

24-JUL-1981 16:11:05.26

NUMBER OF ZERNIKE POLYNOMIALS = 15 NUMBER OF ITERATIONS = 100 ACTUAL NUMBER OF ITERATIONS = 30

			INP	UT P	SF				ESTIMATED PSF								
-2	-2	-6	- 5	1	- 8	0	-2	0	0	0	2	7	3	1	0		
0	5	30	38	32	3	2	4	1	0	0	12	33	7	2	1		
-13)	-12	41	220	25	15	14	1	1	2	39	204	19	6	2		
-12	11	-1	87	353	80	-29	5	0	0	2	78	345	69	7	1		
4	9	4	65	93	63	-6	-2	0	1	1	53	93	51	1 4	2		
2	-23	5	14	31	16	4	17	2	1	0	1	1	4	6	4		
-1	-7	33	35	50	1	-17	-11	o	0	0	1	1	1	1	0		
-7	-4	-8	0	-19	-31	-8	-28	0	0	0	1	2	1	1	0		

MEAN SQUARE ERROR = 12927.4395

K	P(K)
1	0.00000
2	-0.57599
3	0.14083
4	0.09045
5	0.21900
6	0.22991
7	-0.17272
8	0.24472
9	-0.21831
10	0.06116
11	-0.04909
12	-0.15268
13	0.16786
14	-0.02360
15	-0.17726

Figure 57. Blind test results for case 1, $2\lambda F \#$, 15 polynomials

PHRUN25.LUG;1 24-JUL-1981 16:11:05.26 ESTIMATED PHASE ABERRATION (100 = DNE WAVE)

90 105 117 127 134 98 104 109 111 110 Я **-1**3 -5 -8 - 3 -22 -11 -2 - 3 -8 -12 -13 -12 -32 -15 -4 -3 -8 -12 -14 -11 -44 -23 -8 -10 -11 -34 -14 - 2 -51 -26 -46 -25 -11 -2 -9 -11 -13 -10 - 1 -52 -34 -25 -21 -21 -24 -26 -27 -23 -11 -60 -54 -52 -53 -54 -53

HMS PHASE ACROSS APERTURE = 0.362 (WAVES)

Figure 58. Blind test results for case 1, $2\lambda F \#$, 15 polynomials

PHRUN25.LOG; 1

28-JUL-1981 16:23:00.68

NUMBER OF ZERNIKE POLYNOMIALS = 8 NUMBER OF ITERATIONS = 100 ACTUAL NUMBER OF ITERATIONS = 33

	INPUT PSF									ESTIMATED PSF							
-2	-2	-6	-5	1	- B	0	-2		0	1	1	10	4	0	0	0	
0	5	30	38	32	3	2	4		0	0	1	35	35	1	0	0	
-13	c	-12	41	220	25	15	14		1	1	2	34	206	11	5	1	
-12	11	-1	87	353	80	-29	5		1	2	14	95	347	95	1	0	
4	9	4	65	93	63	-6	-2		1	1	2	21	116	26	. 0	0	
2	-23	5	14	31	16	4	17		0	0	0	0	4	2	0	0	
-1	- 7	33	35	20	1	-17	-11		0	0	0	1	1	1	0	0	
- 7	- 4	-8	0	-19	-31	-8	-28		0	0	1	2	1	1	0	0	

MEAN SQUARE ERROR = 15518.1748

K	P(K)
1	0.00000
2	-0.72672
3	0.36828
4	0.09200
5	0.48953
6	0.28294
7	-0.13445
Я	-0.10324

Figure 59. Blind test results for case 1, $2\lambda F\#$, 8 polynomials

-5

-94 -81 -67 -54 -40 -28 -16 ~6 -86 -71 -57 -43 -29 -18 ~7 -75 -60 -45 -31 -19 -9 -1 **-48 -34 -22 -12 -3**

RMS PHASE ACROSS APERTURE = 0.486 (AAVES)

Blind test results for case 1, Figure 60. 2λF#, 8 polynomials

28-JUL-1981 13:26:43.47

NUMBER OF ZERNIKE POLYNOMIALS = 23 NUMBER OF ITERATIONS = 100 ACTUAL NUMBER OF ITERATIONS = 28

			INP	JT P	SF					EST	TAM	ED PS	F		
2	4	-4	-11	-6	-3	-10	1	0	0	0	0	2	2	0	0
8	-25	5	9	11	8	-13	19	0	0	0	0	9	6	0	0
-3	20	-21	-24	75	20	5	10	0	1	1	3	65	23	1	0
-8	8	12	130	251	39	4	12	0	1	13	123	245	30	2	0
6	-13	59	219	164	9	-12	50	1	5	46	215	156	15	1	0
3	14	14	3	32	0	-6	18	3	7	7	7	27	4	1	1
-4	33	~ 5	-16	25	0	17	4	1	1	1	0	4	2	1	1
6	29	-11	-ġ	-18	-16	-21	3.	0	0	0	0	1	1	0	0

MEAN SQUARE ERROR = 9870.0830

К	P(K)						
1	0.00000						
2	-0.21956						
3	-0.10900						
4	0.15145						
1 2 3 4 5	0.07393						
6	-0.26152						
7 8	-0.04469						
R	0.23940						
9	-0.02488						
10	0.14144						
11	0.04048						
12	0,03028						
13	-0.07496						
14	0.06684						
15	0,06582						
16	0.07916						
17	-0,20647						
18	-0.08788	Figure	61	Dlind	test results for	a260	2
19	-0.00951	rigure	01.			Case	۷,
20	-0,01193			2 A F # ,	23 polynomials		
21	0.07280						
22	-0.00148						
23	-0.03374						
2 3	-0.03374	9.6					

28-JUL-1981 13:26:43.47 PHPHN25. LAG:1 ESTIMATED PHASE ABERRATION (100 = ONE WAVE) -8 -2 -5 -14 -17 -14 -7 -18 -22 -21 -14 -6 -17 -24 -25 -20 -3 -14 -22 -25 -22 -13 0 -10 -18 -22 -21 -14 -6 -13 -17 -16 -10 -7 -9 - 3 i -1 - 3 -2 -1

0.213 (#AVES)

Figure 62. Blind test results for case 2, $2\lambda F\#$, 23 polynomials

RMS PHASE ACROSS APERTURE #

PHRUN25.LOG:1

28-JUL-1981 13:44:53.22

NUMBER OF ZERNIKE POLYNOMIALS = 15 NUMBER OF ITERATIONS = 100 ACTUAL NUMBER OF ITERATIONS = 31

			INP	UT PS	SF					EST:	[MATI	ED PS	F		
2	4	-4	-11	~ 6	- 3	-10	1	0	0	0	0	2	2	1	0
8	-25	5	9	11	8	-13	19	0	0	0	0	10	7	2	1
-3	20	-21	-24	75	20	5	10	0	0	0	3	65	12	3	1
-8	8	12	130	251	39	4	12	0	2	9	126	248	21	2	0
6	-13	59	219	164	9	-12	20	4	15	47	219	166	9	1	1
3	14	14	3	32	0	-6	18	2	2	3	9	24	5	2	2
-4	33	-5	-16	25	0	17	4	0	0	0	0	3	2	2	0
6	29	-11	-9	-18	-16	-21	3	0	0	0	0	1	1	0	0

MEAN SQUARE ERROR = 10553.9707

K	b(K)
1	0.00000
2	-0.19623
3	-0.13809
4	0.19114
5	0.03964
6	-0.42954
7	-0.01990
8	0.04450
9	-0.12483
10	0.24520
11	0.05519
12	-0.03948
13	-0.16192
14	0.11369
15	0.11729
	. •

Figure 63. Blind test results for case 2, $2\lambda F \#$, 15 polynomials

PHRUN25.LOG: 1 28-JUL-1981 13:44:53.22 ESTIMATED PHASE ABERRATION (100 = ONE WAVE) -1 - 3 -5 -5 -2 - 3 -9 -10 -6 -8 -2 ŋ -2 -8 -11 -13 -12 -8 -11 -13 -13 -10 - 3 -2 -3 -7 -9 -11 -12 -11 -6 -2 -3 -3 -1 - 3 -3 -1 -1 -3 **-2** - 3 -1 -1 -1

0.224

(WAVES)

Figure 64. Blind test results for case 2, $2\lambda F\#$, 15 polynomials

RMS PHASE ACROSS APERTURE =

28-JUL-1981 12:23:35.56

NUMBER OF ZERNIKE POLYNOMIALS = 8 NUMBER OF ITERATIONS = 100 ACTUAL NUMBER OF ITERATIONS = 27

			INP	UT P	SF				F	EST	TAM	ED PS	F		
2	4	-4	-11	- 6	-3	-10	1	0	0	0	0	1	2	1	0
8	-25	5	9	11	8	-13	19	0	0	0	1	8	8	3	1
-3	20	-21	-24	75	20	5	10	0	0	1	6	77	24	5	1
-8	8	12	130	251	39	4	12	1	0	1	133	252	32	7	2
6	-13	59	219	164	9	-12	20	1	0	2	221	167	29	7	2
3	14	14	3	32	0	- 6	18	0	0	0	9	16	5	2	1
-4	33	- 5	-16	25	0	1 7	4	0	0	0	1	2	1	1	0
6	29	-11	- 9	-18	-16	-21	3	0	0	0	0	1	1	1	n

MEAN SQUARE ERROR = 14042.0928

K	b(k)
1	0.00000
2	-0.26867
3	~0.35244
4	0.19270
5	0.19999
6	-0.14494
7	-0.04886
8	0.26674

Figure 65. Blind test results for case 2, $2\lambda F\#$, 8 polynomials

		25.U MATE!	• •		ABER	RATI) NC					12:2	3:35.	,56		
						68	12	77	82	88	97					
				45	51	55	57	59	61	65	71	80	94			
			32	39	43	44	44	44	44	45	49	55	67	83		
		19	29	34	36	36	34	31	29	29	30	35	43	57	77	
		1.8	26	30	31	29	25	21	18	15	15	18	24	36	54	
	5	17	25	28	27	24	19	14	9	5	3	4	9	19	35	58
•	5	17	24	26	24	20	15	8	2	- 2	- 5	- 5	- 1	6	21	42
į	5	17	23	24	23	18	12	4	-2	-8	-12	-12	-10	-2	11	31
!	5	15	22	24	22	17	10	2	- 4	-10	-15	-17	-14	-7	4	24
•	4	15	22	23	21	16	10	2	-4	- 11	-16	-18	-16	- 9	2	21
;	2	1 4	21	23	22	17	1 1	3	-3	-10	-14	-16	-15	- 8	3	22
		1.3	20	23	22	1.8	12	6	0	-7	-11	-12	-10	-4	7	
		1)	19	23	23	30	15	9	3	-2	- 5	-6	- 4	3	15	
			1 7	22	23	22	18	13	8	4	1	1	5	13		
				21	24	24	22	18	15	12	10	1 2	16			
						26	25	24	22	21	21					
RMS	p	HASE	ACR	oss	APER	TURE	=	c	. 231	. (+	VAVES	5)				

Figure 66. Blind test results for case 2, $2\lambda F\#$, 8 polynomials

NUMBER OF ZERNIKE POLYNOMIALS = 23 NUMBER OF ITERATIONS = 100 ACTUAL NUMBER OF ITERATIONS = 21

			INP	UT P	SF					ESTI	ATE	O PSE	0 0 0 0 0 1 0 0 77 2 0 0 0 250 9 1 0 0 0 0 0							
-5	- 5	-18	8	-3	-1	8	-19	0	0	0	0	0	0	0	0					
-12	71	-8	-24	33	13	37	-19	0	0	0	1	1	0	0	0					
-19	35	-110	-5	207	-19	13	1	0	0	0	2	77	2	0	0					
-11	-49	10	29	381	55	-17	68	0	0	0	7	250	9	1	0					
8	9	70	15	122	7	-5	81	0	0	0	1	4	0	0	0					
-14	31	-22	-53	56	-36	13	4	0	0	0	0	0	0	0	0					
-9	-25	16	-17	4	-85	-95	-42	0	0	0	0	0	0	0	0					
-13	-44	-38	51	-61	-63	-34	-76	0	0	0	0	0	0	0	0					

MEAN SQUARE ERROR = 143020.9531

κ	P(K)						
1	0.00000						
2	-0.96808						
3	0.44031						
4	0.00094						
5	0.00295						
6	-0.00611						
7	-0.03005						
8	-0.00654						
2 3 4 5 6 7 8	-0.06176						
10	-0.04902						
11	-0.00080						
12	-0.00158						
13	-0.00516						
14	-0.00155						
15	-0.00162						
16	0.03939						
17	0.00549						
18	0.02958	Figure	67.	Blind	test results for	case	3,
19	0.00728			2λF#,	23 polynomials		
20	0.04183						
21	0.01596						
22	0.00012						
23	-0.00040						

28-JUL-1981 14:59:21.27 PHRUN25.LOG; 1 ESTIMATED PHASE ABERRATION (100 # ONE WAVE) 95 100 104 99 102 -19 -11 -4 -31 -23 -16 -10 -41 -34 -27 -21 -15 -9 -3 43. -50 -43 -37 -31 -25 -19 -13 -7 -2 -58 -52 -46 -41 -35 -29 -23 -18 -12 -6 -66 -61 -56 -51 -45 -40 -34 -29 -23 -18 -12 -7 - 1 -71 -67 -62 -57 -52 -47 -42 -36 -31 -26 -20 -15 -1 -83 -79 -75 -71 -66 -61 -56 -51 -46 -41 -36 -30 -24 -16 **-92 -88 -84 -80 -76 -71 -66 -61 -57 -51 -46 -39** -101 -98 -94 -89 -85 -80 -,5 -71 -66 -60 -103 -99 -94 -90 -85 -80

Figure 68. Blind test results for case 3, $2\lambda F\#$, 23 polynomials

RMS PHASE ACROSS APERTURE = 0.541 (WAVES)

28-JUL-1981 14:35:45.57

NUMBER OF ZERNIKE POLYNOMIALS = 15 NUMBER OF ITERATIONS = 100 ACTUAL NUMBER OF ITERATIONS = 25

			INP	9 TU	SF				FATIMATED PSF 0 0 0 0 0 0 0 0 0 0 0 0 0 2 1 0 0 0 0 0 2 77 2 0 0 0 0 1 8 247 6 0 0 0 0 0 1 6 2 0 0								
- 5	- 6	-18	8	- 3	- 1	8	-19	0	0	n	0	0	0	0	0		
-12	71	-8	-24	33	13	37	-19	0	0	0	0	2	1	0	0		
-19	36	-110	-5	207	-19	13	1	0	0	0	2	77	2	0	0		
-11	-49	10	29	381	55	-17	68	0	0	1	8	247	6	0	0		
A	9	70	15	122	7	-5	91	0	0	0	1	6	2	0	0		
-14	31	-22	-53	56	-36	13	4	0	0	0	0	0	0	0	0		
-9	-25	16	-17	4	-85	-95	-42	0	ŋ	0	0	0	0	0	0		
-13	-44	-38	51	-61	-63	-34	-76	0	0	0	0	0	0	0	0		

MEAN SQUARE ERROR = 143689.0156

K	P(K)
1	0.00000
2	-0.94646
3	0.27765
4	0.06029
5	0.12885
6	-0.00213
7	0.01058
8	0.01554
9	-0.02690
10	0.04606
11	-0.02607
12	-0.04588
13	0.00858
14	-0.04661
15	0.01193

Figure 69. Blind test results for case 3, $2\lambda F\#$, 15 polynomials

28-JUL-1981 14:35:45.57 PHRUN25.GUG:1 ESTIMATED PHASE ABERRATION (100 = ONE WAVE) 94 100 105 110 115 119 99 103 107 111 114 96 100 103 55/ -7 - 3 -18 -14 -11 -7 -4 -1 -28 -25 -22 -19 -16 -13 -10 -7 -1 -37 -34 -31 -29 -26 -23 -20 -17 -14 -11 -8 -5 - 1 -46 -43 -40 -38 -35 -32 -29 -26 -23 -20 -17 -13 -10 - 3 -6 -51 -49 -46 -43 -41 -38 -34 -31 -28 -24 -20 -17 -13 -60 -58 -55 -52 -49 -46 -42 -39 -35 -31 -27 -23 -18 -14 -68 -65 -62 -58 -55 -51 -47 -43 -38 -33 -29 -24

-77 -73 -70 -65 -61 -57 -52 -47 -41 -36

-84 -80 -75 -69 -64 -58

RMS PHASE ACROSS APERTURE = 0.506 (WAVES)

Figure 70. Blind test results for case 3, $2\lambda F \#$, 15 polynomials

28-JUL-1981 14:45:12.10

NUMBER OF ZERNIKE POLYNOMIALS = 8 NUMBER OF ITERATIONS = 100 ACTUAL NUMBER OF ITERATIONS = 18

	INPUT PSF								ESTIMATED PSF								
-5	- 6	-18	8	-3	-1	8	-19		. 0	0	0	0	0	0	0	0	
-12	71	-8	-24	33	13	37	-19		0	0	0	0	1	0	0	0	
-19	36	-110	-5	207	-19	13	1		0	0	0	3	76	4	0	0	
-11	-49	10	29	381	55	-17	68		0	0	0	6	251	7	0	0	
8	9	70	15	122	7	-5	81		0	0	0	1	3	1	0	0	
-14	31	-22	-53	56	-36	13	4		0	0	0	0	0	0	0	0	
-9	-26	16	-17	4	-85	-95	-42		0	0	0	0	0	0	0	0	
-13	-44	-38	51	-61	-63	-34	- 76		0	0	0	0	0	0	0	0	

MEAN SQUARE ERROR = 143503.1094

K	P(K)
1	0.00000
2	-0.98760
3	0.37287
4	-0.00100
5	-0.00231
6	-0.00026
7	0.02823
8	0.00475

Figure 71. Blind test results for case 1, $2\lambda F\#$, 8 polynomials

ESTIMATED PHASE ABERRATION (100 = ONE WAVE) 97 101 -5 -17 -11 -6 -1 -29 -24 -19 -14 -9 -4 -41 -36 -31 -27 -22 -17 -13 -8 -4 -53 -48 -44 -39 -35 -30 -26 -21 -17 -12 -7 - 3 -5 -65 -61 -56 -52 -47 -43 -39 -34 -30 -25 -20 -15 -10 -73 -68 -64 -60 -56 -51 -47 -42 -38 -33 -28 -23 -17 -12 -84 -80 -76 -72 -68 -64 -59 -55 -50 -45 -40 -34 -29 -23 -92 -88 -84 -80 -75 -71 -66 -62 -57 -51 -46 -40 -99 -95 -91 -87 -82 -78 -73 -68 -62 -57 -102 -98 -93 -88 -83 -78

28-JUL-1981 14:45:12.10

RMS PHASE ACROSS APERTURE = 0.536 (MAVES)

PHRUN25.LUG:1

Figure 72. Blind test results for case 3, $2\lambda F\#$, 8 polynomials

Notes Added in Revision January 27, 1982

The results of our phase estimates, pages 62 to 97, were given to V. Mahajan of Draper Labs on August 14, 1981. Several problems with our data were identified by Draper personnel when they tried to reconcile our phases with their input phases. Our Zernike polynomials are unnormalized (the search does not require normalized polynomials), there is an apparent handedness difference, and our phase array is defined on a 16x16 grid whereas the Draper phase is defined on a 21x21 grid. These differences made it impossible to show that the phase estimation algorithm was working correctly.

In view of these difficulties, we (Draper and EIKONIX personnel) decided to attempt a reconciliation of the differences in software and to have EIKONIX perform another round of testing, this time without a blindfold. Thus we rewrote our software to produce a point spread function based on a 21x21 grid for the phase and to sort out the handedness problem.

We buffered the 21x21 grid (in the spatial frequency domain) with zeroes to form a 64x64 grid. Then we used a 2-D, 64x64 FFT to compute a coherent impulse response, squared the samples, and averaged them with a 6.5x6.5 detector. This produced a 9x9 array from which we selected an 8x8 array to be used as the observed point spread function.

This procedure approximated the way that Draper produced the 8x8 PSF array. The major difference is that they buffer the 21x21 array to 128x128, Fourier transform the array, square the samples, and use a 13x13 detector. Also, the 13x13 detector size is realized by frequency domain multiplication, which requires another pair of 128x128 Fourier transforms. Since we use this procedure so often during our phase estimation search, we could not afford to use the larger (128x128 vs. 64x64) array or calculate the second pair of transforms.

Next, we sorted out the handedness problem. This was done by putting the actual Draper phase into our algorithm described above. It was immediately obvious that an x-y inversion existed and that our y and Draper's y were defined in opposite senses. We modified our software to rectify this problem.

In Figure 73 we show the Draper phase and in Figure 74 we show the Draper PSF and the EIKONIX PSF. The differences in Figure 74 are so slight that we proceeded with confidence into the phase estimation algorithm.

First we performed phase retrieval on the noiseless PSF (the PSF on the left in Figure 74). Since we are no longer blind, we are able to see how well the estimation is done at each step in the search. The results are summarized in Figure 75. Starting at an all-zero phase assumption we find the best 6-parameter phase (an unimportant constant phase, two tilts, and 3 quadratic terms); then, starting at this solution, we find the best 10-parameter phase, etc., to 15 and to 23 parameters.

It interesting to note that the final rms phase difference between the estimated and actual phase is 0.0542 waves. In discussion with Draper personnel, we find that this is approximately the same error that one calculates when a polynomial of this size is fitted directly to the phase itself. Thus, we conclude that phase retrieval on the noiseless PSF was successful. Our estimated phase is shown in Figure 76.

Next we repeated phase retrieval for the first noisy PSF, Figure 34(a). This was derived from the same Draper phase but noise is added to the PSF. We calculated the rms phase difference between actual and estimated by normalizing both phases. We calculated the constant and set of tilts that minimized the rms phase of each, then calculated the difference. The results are summarized in Figures 77 and 78.

Figure 77 shows that the best results are obtained with only 10 parameters. Apparently, for more parameters the algorithm starts to use the extra degrees of freedom to fit the noise. Since the metric (MSE) is available for inspection and since the expected noise variance may be known, this implies that one could continue using more parameters in the search until the expected residual MSE is achieved. There the search would be terminated.

We note that for this noisy PSF the expected MSE is

MSE = (# of PSF samples) (noise variance)

= 64 (2% of DL-PSF peak) 2

 $= 64 (0.02 * 835)^{2}$

= 17,848

and the algorithm yields a MSE that drops from 18,277 to 15,494 as the number of parameters is increased from 6 to 10. Thus 10 parameters is a reasonable stopping point.

Finally we repeated the phase retrieval algorithm on the second, noisy PSF. The results are given in Figures 79 and 80.

In summary, the phase retrieval algorithm was reworked so that there is no effective miss-match between the Draper and EIKONIX software. The polynomials are still different but the manner in which a given polynomial-generated phase is converted to a PSF is the same. The algorithm then yielded a phase that leaves a residual of about 0.1 waves between the actual and estimated phases, when the input PSF is undersampled by a factor of 4 in both x and y directions and when there is a 2% noise on the measured, undersampled PSF.

-12 -22

-10

ï

~

#

-31 -32 -50 -45 -37 -37 -57 -47 -37

-65

Input Phase from Draper Labs Figure 73.

~

0	1	1	1	5	2	2	1	0	1	1	1	5	2	2	1
1	2	2	3	24	7	2	2	1	1	2	. 3	25	Ą	3	2
0	2	2	4	164	28	4	2	0	2	2	4	162	28	4	2
1	3.	5.	51	372	31.	4	2	1	3	5	51	372	32	4	2
1	2	10	53	110	33	4	2	1	2	10	53	111	33	4	2
1	. 1.	2	2	7	5.	2	2	1	1	2	2	7	5	2	2
1	1.	1	2	1	1	1	1	1	1	1	2	1	1	2,	1
0	٥	1	0	1.	1	1	0	0	0	1	0	1	1	1	0
			(;	a)							(b))			

Figure 74. (a) Noiseless PSF from Draper Labs
(b) EIKONIX generated PSF

# of Parameters	MSE Between PSF's	Residual RMS Phase
6	2023	0.0795
10	839	0.0573
15	130	0.0566
23	76	0.0542

Figure 75. Phase Retrieval Summary for the Noiseless PSF

-18 -5 -13 -24 -38 -6 -16 -28 -13 -9 -20 -12 -21 -32 -45 -12 -22 -34 . -8 -14 -21 -31 -43 -9 -10 -13 -17 -24 -32 -43 ç 19 -37 -30 -25 -22 -21 -22 -24 -29 -36 20 49 21 21 21 4 • 20 22 22 21 19 16 22 20 16 -21 22 15 8 22 20 -39 -29 -22 -16 -12 -10 -42 -33 -26 -21 -16 -13 -10 . 19 23 15 21 23 25 25 24 23 22 19 21 25 25 24 14 16 20 23 25 22 13 -22 23 21 17 1 -35 -25 -17 -12 -35 -24 -16 Ş 19 15 • -32 -21 -11 -20 -11 -6 -19 -10 -21 -11

Figure 76. Phase Retrieval Estimate for the Noiseless PSF (compare to Figure 73)

-52 -44 -37 -32 -28 -25 -22 -20 -18 -17 -16 -16 -17

-58 -52 -46 -42 -39 -36 -34 -32 -31

-60

			INP	JT PS	i F			ESTIMATED PSF									
-18	-9	÷5	-11	33	13	-7	-15	0	D	1	4	4	1	1	0		
6	1	27	33	30	4	-3	0	0	1	1	13	24	1	0	0		
-45	-15	2	29	179	12	27	0	0	1	1	24	171	2	1	0		
14	~2	6	66	352	58	-15	-4	1	1	4	60	340	52	3	1		
-2	12	1	61	95	58	-11	3	1	2	4	53	86	46	1	0		
29	-20	3	16	34	13	5	15	0	0	1	13	17	6	0	0		
-2	-8	26	35	11	-4	-19	-14	0	0	1	2	3	1	0	0		
-16	- A	-12	-R	-15	-30	-6	-25	0	0	1	1	1	0	0	0		

MEAN SQUARE ERROR = 14377.8516

(a)

# of Parameters	MSE Between PSF's	Residual RMS Phase
6	18277	0.0930
10	15494	0.0890
15	14731	0.1030
23	14377	0,1065
	(c)	

Figure 77. (a) First noisy PSF

- (b) Estimated PSF
- (c) Phase Retrieval Summary

• 45

**

```
-6 -13 -16
                                                                                                                                                                                                                            -8 -11 -15 -18 -20
                                            -9 -16 -21 -21
                                                                                                                                                                                                               -7 -10
                              -7 -14 -21 -27 -29
                                                                                                                                                                                                                                           -9 -11 -13 -15 -18 -21 -24 -28 -31
               -33 -33 -29 -24 -19 -15 -14 -15 -18 -23 -29 -34 -37
                                                                                                                                                                                                                                                        -12 -15 -17 -18 -20 -22 -25 -27 -30 -34 -37 -41 -45
                                           ,0
-36 -35 -32 -31 -31 -32 -35 -39 -43
                                                            10
                                                                                                                                                                                                                             Ş
                                                                                                                                     25
                                                                                                                                                                                                                             ~
                              -2
                                            12
                                                           22
                                                                          28
                                                                                                       30
                                                                                                                                                   21
                                                                                                                                                                                                                            7
                                            15
                                                           24
                                                                         30
                                                                                                                                                   20
                                                                                                      30
                                                                                                                                    23
                                                                                                                     27
                                                                                        3
                                                           24
                                                                         59
                                                                                        30
                                                                                                      53
                                                                                                                     56
                                             15
                                                                                                                                    22
                                                                                                                                                   19
                                                                                                                                                                 16
                                                                         56
                                                                                                       56
                                                                                                                                                                 9
                                                                                        28
                                                                                                                     24
                                                           21
                                                                                                                                    21
                                                                                                                                                                                                                                           8
                                                                                                                                    19
                              7
                                                                                                                                                                                                                                            9
                             -31 -31 -26 -19 -11
                                            6
                                                                                                                                                                                                                                            .
                                                                                                                                                                                                                                            Ť
                                                                          ~
                                            -26 -29 -26 -18
                                                           -26 -25 -19 -10
                                                                                                                                    10
                                                                                                                                                                                              10
                                                                                                                                                                                                                                           ?
                                                                         -17 -22 -20 -12
                                                                                                                                                                                10
                                                                                                                                                                                              10
                                                                                                                                                                                              10
                                                                                        -14 -18 -14
                                                                                                      -10 -12
                                                                                                                                                                                                                            Ξ
                                                                                                                                    12
```

Figure 78. Phase Retrieval Estimate for the First Noisy PSF (compare to Figure 73)

-31 -34 -36 -39 -42 -45 -49 -53 -57

			INP	UT P	SF					1 0 1 4 3 1 0									
26	-3	5	44	-13	-4	27	-22	0	0	0	0	1	1	0	0				
-22	-33	4	21	11	5	-8	18	0	1	0	1	4	3	1	0				
2	13	-11	-29	56	14	6	9	0	1	1	2	53	17	2	1				
-10	3.	10	102	240	29	13	1	0	1	12	101	235	26	3	1				
-15	-13	41	209	164	5	-8	21	1	2	40	207	161	8	1	0				
-2	11	16	-6	31	-2	0	16	1	1	1	4	30	4	1	0				
-9	31	2	-12	20	-3	16	-1	0	1	D	D	2	1	1	0				
-22	24	-0	-17	-21	-16	-25	10	0	0	0	0	1	1	0	ø				

MEAN SQUARE ERROR = 14524,2539

(a)		(p)	
# of Parameters	MSE Between PSF's	Residual RMS Phase	
6	18,655	0.1312	
10	16,486	0.1039	
15	14,913	0.0944	
23	14,524	0.1062	
	(c)		

- Figure 79. (a) Input PSF
 - (b) Estimated Phase
 - (c) Phase Retrieval Summary

-22

-36 -32 -27 -21 -14

-8 -1 ~ --25 -27 -26 -22 -17 -12

-7 -16 -25 -34 -8 -15 -24 ~ -14 -17 -18 -15 -11 • -10

-6 -16 -26 -34

-2 -13 -24 -34 -40 -4 -15 -25 -34 -41

ç

-33

•5 •16 •25 •31

-12 -21 -27

2-

•

6

6

-8 -19 -29 -35

~

0 -11 -22 -32 -38

-5 -11 -16

-9 -16 -21

6

-11

-33 -25 -17

-38 -26 -16

-31 -19

-24 -13

-19

-41 -33 -26 -20 -13

-47 -42 -37 -31 -25 -18 -11 -43 -36 -31 -25 -19 -12

-50 -44 -38 -30 -23 -15

-36

Phase Retrieval Estimate for the Second Noisy PSF (Compare to Figure 73) Figure 80.

-25 -13

DISTRIBUTION LIST

Cape Diris Hamili Radozoosi	J	
RADOZIOLO GRIFFIOS Aro dr 13441	i	2
RACULAR CRIFFL IS And NY 13441	2	3
ADALIOTATOR DEC TECH INF CIR ATINE DITE-DDA CAREROR SIA OS 5	12	5
ALGXANDRIA VA 22314 Elkoniv Corp Attn: ur. Robert Donsavies 23 Crosby Dr. Bedrord, MA U1/30	5	3
Aerospace Corporation Attn: ar. Steve durrin Advanced Systems fechnology Division 2400 c. al Segundoslvd. Bldg 125/1054		4
Lie aerospace Corp. Atuntr. Silvertooth P.). Box 9295/ El Sejando, CA 90009	1	5
Air Force Wright Aeronautical Laboratory File ATIN: Mr. Joseph Johnson Wright Patterson AF3, Oi 45433	1	ó
Airsearch Manufacturing Co. of California Atun: Mr. Oscar Buchmann 2525 Mest 190th Street Forrance, Ch. 90509		7

Analylic Decisions Incorporated Attn: Mr. dicharddollicone 5330 West Rosecrans Avenue Suite 203 Lawndale, CA 22209	i	ઇ
Analytic Decisions, Incorporated Attn: Mr. Gary Glaser 1401 Milson Blvd Arrington, VA 22209	ì	9
Center for Analysis Attn: Mr. Jim Justice 13 Corporate Plaza NNewport deach, CA 92660	1	10
The Charles Stark Draper Laboratory, Inc. Attn: Jr. Keto Soosaar 550 fechnology Square Cambrioge, MA 02139	1	11
Charles Starke braper Labs Attn: br. V. Manajan 555 Technology Square MS-85	1	12
Cambridge, MA 02139 DARPA/STO Attn: Maj E. Deitz 1400 N.lson Blvd Arrington, VA 22209	1	13
DARPA/STO Attn: Lt. Col A. Herzberg 1400 Wilson Blvd Arlington, VA 22209	1	14
DARPA/LEO Atun: Col R. Prater 14.00 Hilson Blvd Arrington, VA 22209	1	15
JARRAZAIS 1400 Allson divd Arlington, VA 22209	1	16

Eastman Kouak Co. Aton: Richard Frice Ku- Lincoln Plant 901 Elagrove Rd. Rochester, N.Y. 14550	ł	17
Santa Sarpara, CA 93105	t	13
General Research Corporation Attn: Mr. Chomas Zakrzewski 7055 Old Springhouse Road McLean. VA 22101	į	19
nujhes Aircraft Company Attn: Mr. Ken deale Centinela & feale Streets Curver City, CA 90230	1	20
dupmes Aircraft Company Attn: Fritz denning MS 6/2 120 Centingla & Feal Sts Culver City, CA 90230	l	21
Institute of Defense Analyses Attn: Dr. Hans Wolfhard 400 Arny Javy Srive Arlington, VA 22202	. 1	22
Itek Corporation Atom: Mr. Edward Calat 10 Maguire Road Lexington: MA 021/3	1	23
Kanan Sciences Corporation Attn: Dr. Halter D. Hare 1500 Garden of Sous Road P.). Dox 1463 Cororado Springs, On 80233	1	24
Lockhaed missiles a Space Company Aton: Mr. Paul Milliamson 3251 Manover Street Paro Arto, Ca 94301	ł	26

Naval electronic Systems Command PML-100-4. Attn: Wr. Charles Jood National Center I Washington, J.C. 20360	i	26
Naval Research Laboratory 20170 Attn: Dr. John Accallin 45.5 Overlook Ave. Sh Hashington, D.C. 20375	I	27
Naval sea Systems Command Attn: Dr. S. Sianityar PhS-405 HCL Room 11.408 Washington, D.C. 20742	1	28
NASA Ares Research Center MS244-7 Modfett Field, CA 74035	l	29
Ortical Sciences co aten: Dr. D. Fried P.O. DOX 446 Plicencia, CA 92670	1	30
rerkin-Elmer Corp nton: Ar. d. Levinstein 100 nooster Heights Ru. Danbury, Ci Oó810		31
Photon Research Associaces Aton: Mr. Jim Myer P.O. Box 1318 La Jolla, CA 92038	1	32
Aiverside Research Aton: HALO Library, Mr. Boo Passut 1701 M. Fort Myer Prive Artington, VA 22209		
Accement International Atom: Aussell Loftman (Space Systems Group) 12214 Lakewood Blvt. Dorney, CA 90241 (mail Code - SL So)	1	34

Schence Applications, Inc. Aben: Mr. Richard Ryan 3 Freston Court Beuford, MA 01730	i	35
Sensor Systems Group Attm: Joseph S. fitus 18: Went Screet Walthar, Wass 0215:	4	36
film Aton: Mr. Len ringus Blug. R-5 Reconcus Bec., CA 90278	1	37
University of Arizona Atom: Robert Shamon % Unaries Reyton Administration Slug. Tuocon. AZ 35721	i	38
J.J. Army/DARCOm Aton: Ar. dernie Chasnov AAC 3129 5001 disenhower Ave Alexanuria, VA 22333	1	39
J.J. Army missile Command Attn:RSml=RAS/Ar. Fred Haak Reustone.arsenal. AL	1	40
Space Livision Attn: Maj T. Fern SD/VLV. P. 0. 92960 Worldway Postal Center Lou Angeles, CA 90009	J	41
RGD Associates, Inc. Atun: Dr. Richard Barakat r.O. Box B Maylano, Ma 01.778	1	42

Edla Attn: Dr. Stan Robinson 2.0. Sox 3518 Ann Arbor, all 48107

Attak Corp.
Atta: John Matson
Optical Systems Division
10 Majrire Rd.
Lexington; MA 02173

du nes Aircraft Co. Attn: Grent Ellerprooke Centenela & Teal Streets Curver City, CA 90230 45

MISSION of Rome Air Development Center

RADC plans and executes research, development, test and selected acquisition programs in support of Command, Control Communications and Intelligence (C³I) activities. Technical and engineering support within areas of technical competence is provided to ESD Program Offices (POs) and other ESD elements. The principal technical mission areas are communications, electromagnetic guidance and control, surveillance of ground and aerospace objects, intelligence data collection and handling, information system technology, ionospheric propagation, solid state sciences, microwave physics and electronic reliability, maintainability and compatibility.

MEMBER CARLAR CARLAR CARCAR CA